[redacted]

NRL Report 5790

UNCLASSIFIED

NRL RESEARCH AND DEVELOPMENT PROGRAM FOR THE FLEET BALLISTIC MISSILE

REPORT OF LONG RANGE RESEARCH FOR NAVY SEA-BASED DETERRENCE

March 1, 1962

DECLASSIFIED: By authority of
OPNAVINST 5510.1H, 29 APR 88
Cite Authority Date
C. ROGERS 1221.1
Entered by NRL Code

APPROVED FOR PUBLIC RELEASE - DISTRIBUTION UNLIMITED

U. S. NAVAL RESEARCH LABORATORY
Washington, D.C.

[redacted]

APPROVED FOR PUBLIC RELEASE
DISTRIBUTION UNLIMITED

[redacted]

[redacted]

[redacted]

[redacted]

UNCLASSIFIED

CONTENTS

PREFACE ii

THE ANALYSIS OF ORGANIC VAPORS IN NUCLEAR SUBMARINE ATMOSPHERES (Unclassified)
R. E. Kagarise and R. A. Saunders 1

RECENT ADVANCES IN GLASS FIBER REINFORCED PLASTIC ROCKET MOTORS ([redacted])
J. A. Kies and H. Bernstein 16

IN SITU HALL EFFECT MEASUREMENTS ON THIN GERMANIUM FILMS (Unclassified)
J. E. Davey and M. D. Montgomery 28

CURRENT FLOW DUE TO MOTION OF CHARGED DISLOCATIONS
W. H. Vaughn (Unclassified) 35

[redacted]

PREFACE

The various Naval laboratories, under sponsorship of the Special Projects Office, have undertaken a program of exploratory scientific investigation calculated to influence the future Navy's at-sea deterrence capability. A program of directed research of some duration is anticipated (and required) to put together elements which are fundamental to the formulation of a future sea based deterrence weapon systems concept.

An appropriate administrative framework has been established at NRL to sponsor, on a Laboratory-wide basis, the conduct of applicable exploratory research. Investigations, matched to existing NRL scientific programs and skills, have been initiated within this framework. They are broadly directed toward a consolidation of scientific knowledge and technological capabilities applicable to the initiation of a firmly scheduled development by the Navy of a sea based deterrence weapon system matching the operational requirements of its day.

This report is one of a series intended to display the NRL research activity directed to support this follow-on sea based deterrence weapon system concept.

Peter Waterman

Peter Waterman
Staff Adviser for FBM

[redacted]

UNCLASSIFIED

THE ANALYSIS OF ORGANIC VAPORS IN NUCLEAR SUBMARINE ATMOSPHERES

R. E. Kagarise and R. A. Saunders
Chemistry Division
(Unclassified)

The Naval Research Laboratory (Chemistry Division) is endeavoring to extend known information about the analysis and control of nuclear submarine atmospheres to the expected long range problems in an FBM submarine of the future. Basic research is being conducted utilizing advanced techniques of molecular spectroscopy and gas chromatography, as well as the development of analytical techniques which may be applied to appropriate submarine atmosphere problems. . . . . FBM Staff

INTRODUCTION

With the advent of nuclear-powered submarines and their inherent capability of extended submergence times, an urgent need arose for methods of monitoring and analyzing submarine atmospheres. The problem may be divided into two parts: the analysis of major atmospheric constituents and the analysis of minor atmospheric constituents. Under the category of major constituents one finds such compounds as oxygen, nitrogen, carbon dioxide, hydrogen, water vapor, carbon monoxide, methane, and Freon-12 (dichlorodifluoromethane). The importance of many of these compounds is attested to by the large amount of equipment devoted to their control and measurement, such as the MEA CO_2 scrubber, the Desomatic H_2-CO burner, and the Mark III Atmosphere Analyzer (1,2). The air conditioning equipment, in addition to its primary function of temperature control, is also effective in controlling the relative humidity of the submarine atmosphere.

Present analytical methods are generally adequate for the monitoring of the major atmospheric constituents. This is not to say that improvements cannot be made, however, and the Navy is currently developing the Mark IV Atmosphere Analyzer. Research is also being conducted to determine the feasibility of using gas chromatography for the routine monitoring of O_2, N_2, H_2, CO_2, Freon-12, CO and CH_4.

The second category of atmospheric constituents, the minor constituents, are primarily pollutants, since their presence is neither essential nor desirable in an ideal atmosphere. These pollutants include particulate matter, aerosols, and a wide variety of organic vapors. The concentration of these materials will vary considerably, depending upon the past history of painting, the current use of cleaning solvents, the level of smoking, and the manipulation or abuse of fuels and oils. The total level of contamination due to the organic vapors and gases falls in the 5 to 15 parts per million (ppm) range for most of the currently operating nuclear boats.. Of course, unusual conditions can produce levels which fall outside of this average range. When one considers that high resolution vapor phase chromatograms of this material indicate the presence of over 100 different compounds, the difficulties involved in identifying individual compounds are apparent. This report will deal with recent efforts of the Chemical Spectroscopy Section, Physical Chemistry Branch of the Chemistry Division in developing analytical methods to cope with this exceedingly complex analysis.

[redacted]

COLLECTION OF SAMPLES

The prerequisite to any successful analytical scheme is the procurement of a sufficient amount of reasonably pure material upon which to conduct the analysis. Since one is primarily concerned with the analysis of the minor constituents, the presence of the major constituents is undesirable. Thus, the primary sample, i.e., the submarine atmosphere, consists of 5-15 parts of usable sample diluted with a million parts of uninteresting and/or interfering material, namely the oxygen, nitrogen, water vapor, and carbon dioxide of the normal atmosphere. Thus, the direct analysis of submarine atmospheres, either by infrared spectroscopy or gas chromatography, has only been successful for those constituents which are present at concentrations greater than approximately 5 ppm. Since this is near the total concentration level of the minor constituents, this approach is not feasible for the identification of trace contaminants, and one must resort to concentrating schemes.

Two possible methods of concentrating trace contaminants appear practical for submarine usage: (1) freeze-out and (2) adsorption. The first approach has been tried, but with limited success. The large amounts of water and CO_2 collected by this method tend to limit its sensitivity and therefore its usefulness. The use of adsorption techniques, on the other hand, has been more successful. The best absorbent for this purpose is activated carbon which possesses the ability to adsorb a wide spectrum of organic materials, yet at the same time does not adsorb water too strongly. The sample collecting procedure most commonly employed at the present time consists of the following steps: activated carbon is exposed aboard the submarine by forcing air through it at the rate of 5 cfm for a period of time ranging from several hours to 24 hours. If exposure times become too long, the carbon becomes preferentially saturated with higher-boiling materials which displace the lower boiling compounds previously adsorbed by the carbon.

The exposed carbon is then returned to the laboratory for desorption and subsequent analysis of the desorbate. Two methods of desorption are commonly employed, vacuum desorption and steam elution. In the first method, the carbon is slowly heated in an evacuated system to a temperature of about 300°C. The desorbed materials are collected in traps cooled with liquid nitrogen. The virtue of this method is the ease with which the lower boiling desorbents can be retained, at the expense of not recovering all of the higher molecular weight materials. In the steam elution technique, the carbon is subjected to a stream of high pressure steam. The combined action of the heat and the displacing power of the water effectively removes a large portion of the adsorbed materials. The disadvantage of this method lies in the fact that materials which are gases or volatile liquids at room temperature are difficult to retain. In addition, the desorbate is contaminated with a copious quantity of water which tends to dilute any water soluble contaminants in the original atmosphere.

Since current interest has centered upon the lower molecular weight materials, the vacuum desorption method has been used almost exclusively by the Chemical Spectroscopy Section. After desorption, the total desorbate is crudely separated into three fractions: a vapor phase, consisting primarily of materials which are gases at room temperature; an oil phase, consisting mainly of aliphatic and aromatic hydrocarbons; and an aqueous phase, made up of water and water-soluble organic compounds.

It should be pointed out that the carbon adsorption-desorption method of sampling possesses several deficiencies which limit its usefulness. In the first place, it is virtually impossible to determine the adsorption-desorption efficiency for any given compound in such a complex mixture and at the low concentration levels commonly experienced. Thus, any analysis based on activated carbon as the sample collecting medium is, of necessity, qualitative. Concentration values must therefore be understood as being minimal values and are usually based on an adsorption-desorption efficiency of 100%. Secondly, the adsorption-desorption process may alter the character of a contaminant through decomposition or chemical reactions. The extent of such changes are not known and considerable research remains to be done on this aspect of the problem.

UNCLASSIFIED

ANALYSIS OF MATERIALS

As stated previously, the minor contaminants of a typical nuclear submarine atmosphere constitute an exceedingly complex mixture of organic materials. At first glance, gas chromatography might appear to be the most promising technique for the solution of this problem. Columns of extremely high resolving power are available to separate the multitude of compounds, and hydrogen flame and β-ray ionization detectors possess the sensitivity needed to detect the small amounts of trace materials encountered. However, gas chromatography possesses one inherent shortcoming which seriously negates its advantages, namely, its lack of specificity. This is to say that several compounds may pass through the column with the same retention time. If one is working with a homologous group of compounds this shortcoming is not serious. However, when an unknown may consist of aliphatic, olefinic and aromatic hydrocarbons, ketones, alcohols, acids, etc., the lack of specificity becomes very serious indeed. One approach to this problem is to combine the separatory powers of gas chromatography with the specificity of a second analytical method such as infrared and/or mass spectroscopy. A considerable amount of research has been conducted during the past year to afford an efficient wedding of these various techniques. In particular, we have been concerned with the use of infrared spectroscopy as the identifying technique, even though it is somewhat less sensitive than mass spectroscopy. Infrared spectroscopy was chosen because it is somewhat more specific than mass spectroscopy and because a more extensive catalog of reference spectra was available.

Two basic problems had to be solved in order to apply the combined techniques of gas chromatography and infrared spectroscopy. First, methods for efficiency collecting the various chromatographic fractions had to be developed. While various collecting systems have been described in the literature, none are completely satisfactory. Secondly, the sensitivity of the infrared method had to be maximized by efficient utilization of the very small amounts of sample normally collected.

The fraction collector which has been developed is shown in Fig. 1. The effluent from the gas chromatograph, which consists of the sample plus the helium carrier gas, is passed through the cold collecting tube. The sample is frozen out on the walls of the tube while the helium escapes through the bottom hypodermic needle. The collection efficiency for lower boiling components can be improved by filling the tube with glass chips. After a given peak has been eluted, the tube is removed and replaced with a clean tube and the next peak is collected.

After collection, the sample is introduced into the appropriate infrared absorption cells for analysis. Materials which are gases or volatile liquids at room temperature are introduced into a commercially produced microgas cell. This cell has a path length of 60 cm, while having a volume of only 20 ml. A high path length to volume ratio is desired for maximum sensitivity when dealing with sample-limited analyses. Materials which are liquids at room temperature are studied as liquids. A cell having a variable path length and a very small volume was designed and constructed for this purpose. A schematic diagram of this cell is shown in Fig. 2. The external dimensions are 15 mm × 3 mm × 3 mm. The maximum separation of the plates is 0.3 mm, which yields a total volume of 6.75 microliters (μl). However, satisfactory spectra have been obtained with 0.25 μl samples.

The frozen-out sample is removed from the liquid nitrogen and allowed to melt. The liquid is transferred from the collection tube to the microcell either by gravity flow or by placing the tube and cell in a holder designed for the purpose and centrifuging the liquid out through the bottom needle and into the absorption cell.

Let us now briefly consider the sensitivity of the analytical method. In theory, if one were dealing with a single contaminant, there is no limit to the sensitivity. One simply exposes the carbon until a sufficient amount of material has been collected. Obviously, it is not practical to expose the carbon for extremely long periods such as weeks or months and we shall therefore limit the discussion to twenty-four hour exposures. Using a flow

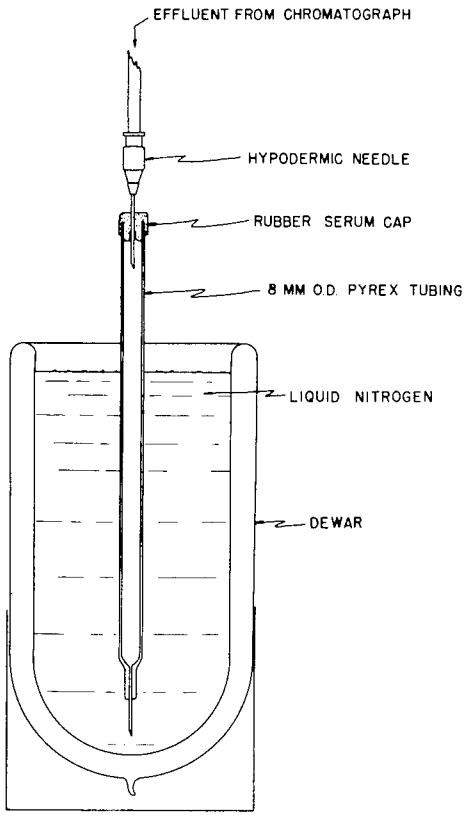

Fig. 1 - Fraction collector

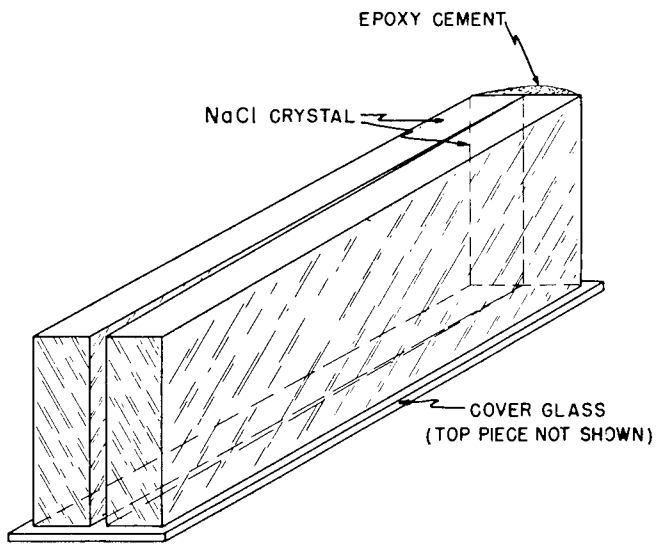

Fig. 2 - Variable path microliquid absorption cell

rate of 5 cfm, a volume of 7200 cu. ft. (or about 242,000 grams) of air is sampled during this period. If one is dealing with strong infrared absorbers such as acetylene, benzene, the Freons, etc., a sample of 10 μg is sufficient to yield a distinguishable infrared absorption spectrum, using the microgas cell. The concentration (by weight) needed to yield this amount of material is given by

$$c = \frac{10 \times 10^{-6} \text{ grams}}{242{,}000 \text{ grams}} = 4.13 \times 10^{-11}$$

or about 4 parts in one hundred billion! By using a gas chromatograph equipped with a hydrogen flame detector, one can further improve this sensitivity by a factor of about 10^4. Of course, the price paid is the specificity of infrared spectroscopy.

It should be stressed that these sensitivity values represent ideal conditions and various practical considerations reduce the limits of detectability. Without going into details, it can be said that a more practical value is roughly 1 part in 10^9. For very weak infrared absorbers this would be reduced considerably. Hydrogen sulfide, for example, cannot be detected at a concentration lower than about 0.1 ppm.

SOME TYPICAL ANALYSES

Having discussed in some detail the sampling and analytical techniques, let us now consider some typical analyses. The samples to be discussed were desorbed from carbon which had been exposed for twenty-four hours aboard the USS TRITON. The desorbed material is very similar to that obtained from other nuclear submarines, including several SSB(N) boats.

[redacted]

UNCLASSIFIED

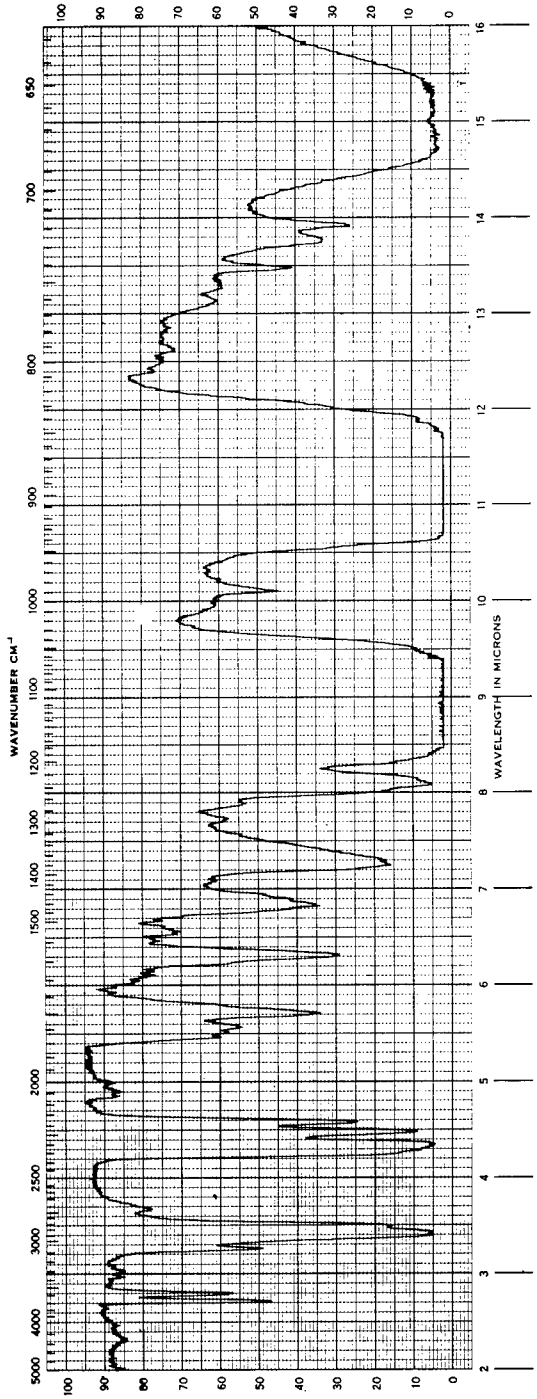

Fig. 3 - Infrared spectrum of whole vapor phase desorbate

The infrared spectrum shown in Fig. 3 is that of the vapor phase desorbate before any separation by gas chromatography. The strong, broad regions of absorption around 9, 11, and 15 microns are due to carbon dioxide and Freon-12, which together make up about 95% of the total sample. The absorption due to these two components masks out practically all of the absorption arising from the other components. The gas chromatogram of the vapor phase desorbate is shown in Fig. 4. The first three peaks are due to air, carbon dioxide, and Freon-12 and probably small amounts of methane, ethane, and ethylene. These peaks have been attenuated by factors of from 50 to 200 with respect to the remaining peaks. The spectrum of the minor components can be studied by collecting only the material eluted after the first three peaks. The spectrum of this fraction is shown in Fig. 5(a). Comparison of this spectrum with that shown in Fig. 3, shows some rather striking differences due to the removal of the CO_2 and CCl_2F_2 (Freon-12). This spectrum (Fig. 5(a)), while vastly improved over the first one, is still complicated by the presence of at least thirteen different compounds. The spectra can be further simplified by collecting the material eluted under individual peaks. Examples of two such spectra are shown in Figs. 5(b) and 5(c). The peak at 4.0 min retention time (Fig. 4) is readily identified as being due to isobutylene, while the peak at 14.8 min is due to isoprene, the monomer unit of natural rubber. The strongest bands of these two compounds are badly overlapped, and it is doubtful whether they could have been identified by infrared spectroscopy alone. Numerous other peaks have been collected and the compounds responsible for them identified by infrared spectroscopy. A typical analysis is given in Table 1 for material collected aboard the USS SNOOK. A number of materials, labeled as unidentified, can only be characterized as to type, e.g., aliphatic hydrocarbon, due to the lack of reference spectra and to the spectral similarity of closely related compounds. However, this is itself valuable information since these compounds are all relatively harmless and can therefore be discounted as being hazardous from a physiological point of view.

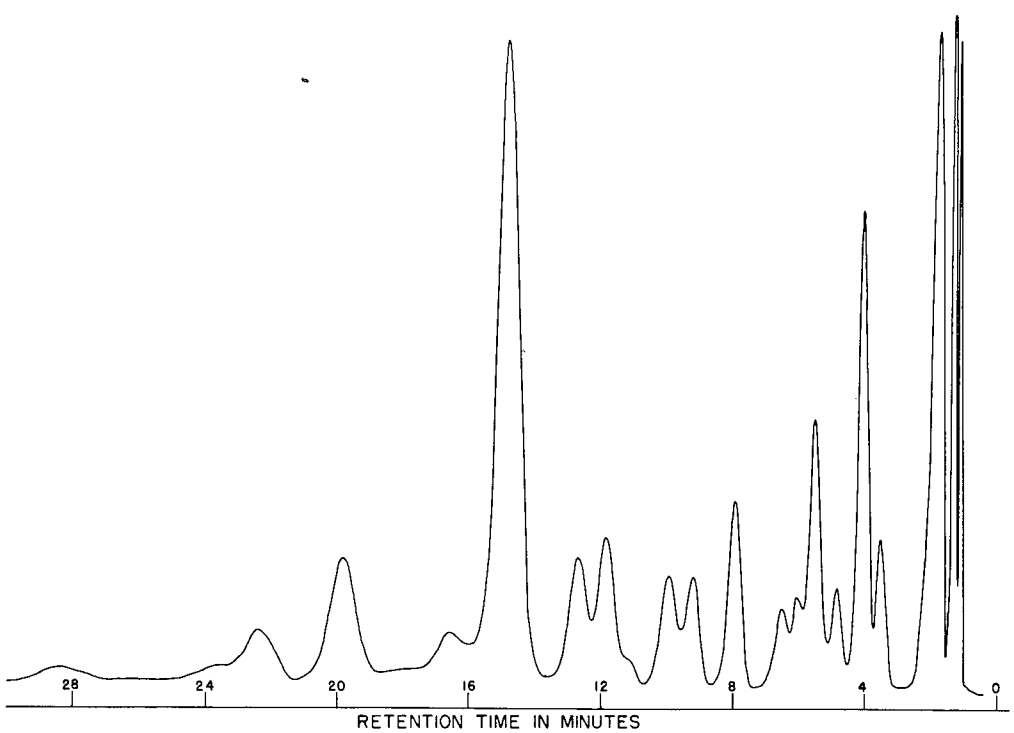

Fig. 4 - Gas chromatogram of whole vapor phase desorbate

UNCLASSIFIED

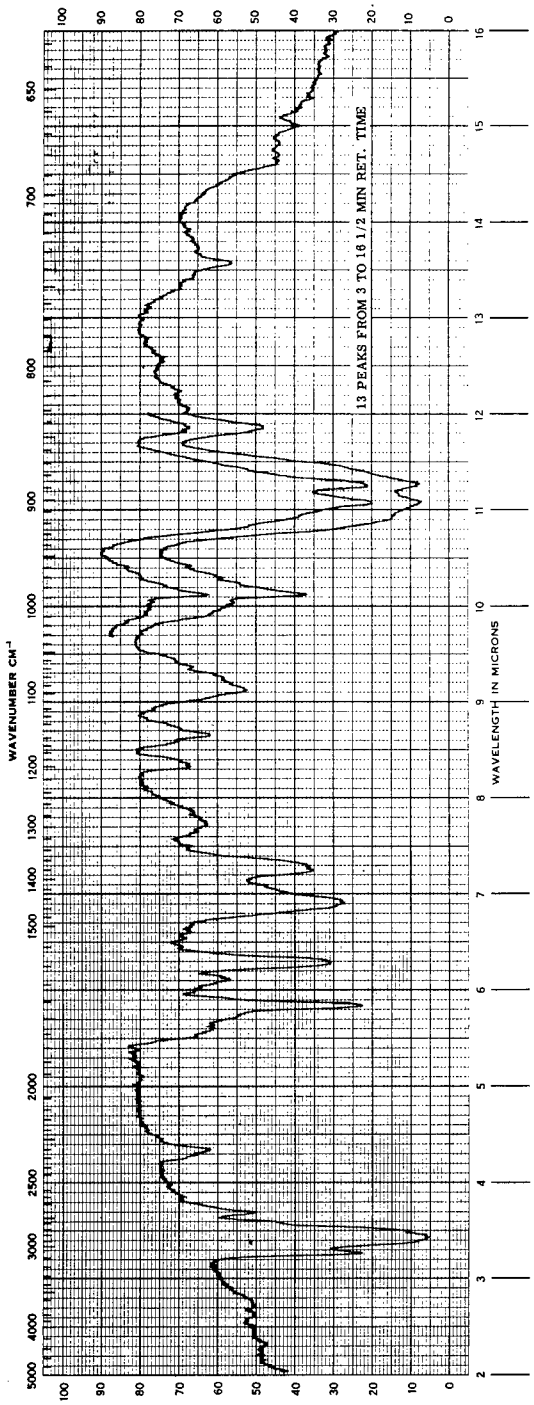

Fig. 5(a) - Infrared spectrum of the material collected under the 13 peaks from 3 to 16-1/2 minutes retention time

[redacted]

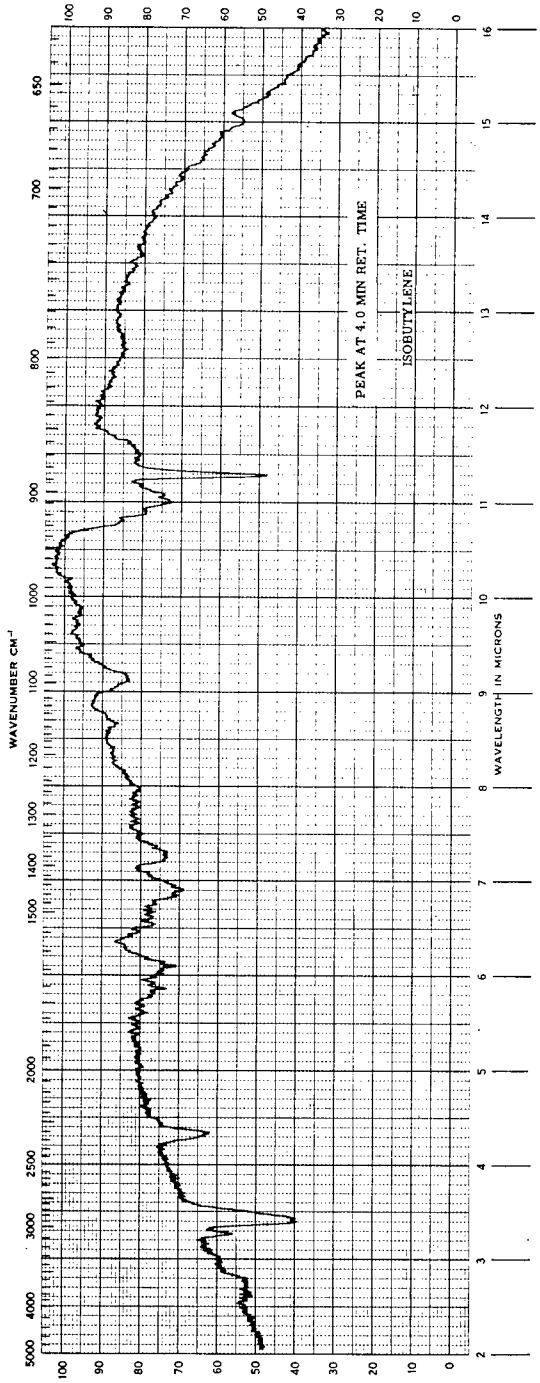

Fig. 5(b) Infrared spectrum of peak at 4.0 minutes retention time

UNCLASSIFIED

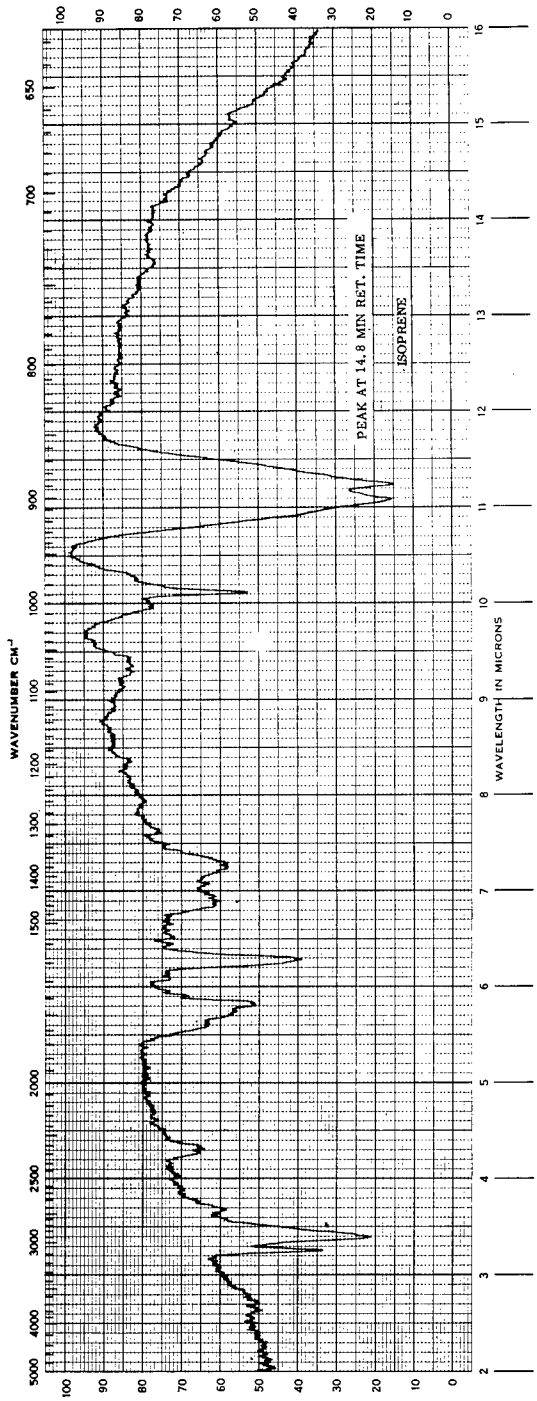

Fig. 5(c) - Infrared spectrum of peak at 14.8 minutes retention time

Table 1
Chromatographic Analysis of C-215 Desorbate
(Volatile Fraction)

Peak No.	Retention* Time	Peak Height	Attenuation Factor	Identity
1	0.57	100	10^5	Methane
2	0.70	53	10^5	Ethane, ethylene
3	1.20	44	5×10^4	Propane
4	1.45	38	5×10^4	Freon-12
5	2.01	36	2×10^4	iso-butane
6	3.08	94	2×10^4	n-butane
7	3.81	57	10^5	iso-butene
8	4.95	3	10^5	2-butene (trans)
9	5.50	4	5×10^3	unidentified
10	6.04	85	5×10^3	2-butene (cis)
11	6.65	68	5×10^4	iso-pentane
12	7.50	6	5×10^4	unidentified
13	9.60	85	2×10^4	n-pentane
14	11.80	60	2×10^4	unidentified
15	13.05	35	2×10^4	unidentified
16	15.25	20	2×10^4	unidentified
17	16.40	12	2×10^4	unidentified
18	17.60	31	2×10^4	unidentified
19	18.60	11	2×10^4	unidentified
20	21.20	61	2×10^4	Isoprene
21	23.90	21	2×10^4	unidentified
22	30.75	86	5×10^3	unidentified
23	34.80	32	5×10^3	n-hexane
24	38.40	65	5×10^3	unidentified
25	52.65	15	5×10^3	unidentified

*12 ft benzyl ether column, 0°C, 30# helium pressure.

UNCLASSIFIED

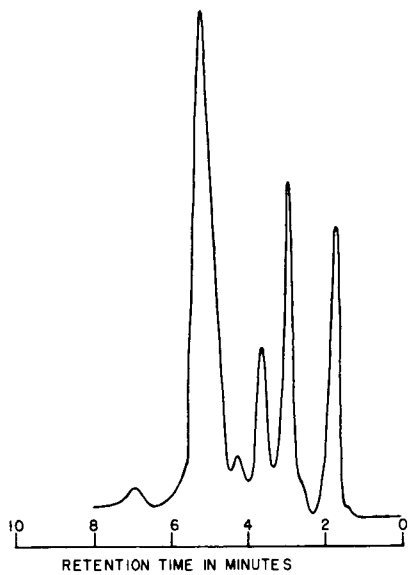

Fig. 6 - Gas chromatogram of aqueous phase desorbate

A second example of how gas chromatography and infrared spectroscopy are used as a team is shown in the analysis of the aqueous phase of the USS TRITON desorbate. In Fig. 6 we have shown a portion of the gas chromatograph of this aqueous phase. These peaks are due to a very small fraction of the total sample, which is more than 99% water. The strongest peak at 5.4 minutes retention time was collected and the infrared spectrum of the eluted material obtained as shown in Fig. 7(a). A comparison of the spectrum with those of ethanol (7b) and isopropyl alcohol (7(c)) shows conclusively that the 5.4 minute peak, which appears to be due to a single compound, is in fact a mixture of these two materials, the major component being ethanol. The other peaks were identified as being due to acetaldehyde, acetone, ethyl acetate, methyl alcohol, and methyl isobutyl ketone.

As a final example of the versatility of infrared-chromatographic approach we have listed in Table 2 all of the compounds which have been identified in nuclear submarine atmospheres by means of this analytical approach. In addition to these compounds, which have been specifically identified, at least thirty other compounds have been characterized as to chemical type, e.g., a C_5-branched aliphatic, a C_8-branched olefin, and a C_5 aldehyde, etc. It should be mentioned that in spite of the length of this list, many compounds still remain to be identified. This has not been achieved to date primarily because of their extremely low concentrations relative to the larger amounts of aliphatic and aromatic hydrocarbons which constitute the bulk of the minor constituents.

Table 2
A Summary of Compounds Identified in Nuclear Submarine Atmospheres by Infrared Spectroscopy and Gas Chromatography

1. methane	20. isoprene	39. carbon monoxide
2. ethane	21. benzene	40. dichlorodifluoromethane (Freon-12)
3. propane	22. toluene	41. dichlorotetrafluoroethane (Freon-114)
4. iso-butane	23. ortho-xylene	42. acetylene
5. n-butane	24. meta-xylene	43. methyl alcohol
6. iso-pentane	25. para-xylene	44. ethyl alcohol
7. n-pentane	26. ethyl benzene	45. isopropyl alcohol
8. n-hexane	27. n-propyl benzene	46. nitrous oxide (N_2O)
9. n-heptane	28. iso-propyl benzene	47. acetaldehyde
10. n-octane	29. n-butyl benzene	48. acetone
11. n-nonane	30. sec-butyl benzene	49. methyl ethyl ketone
12. n-decane	31. tert-butyl benzene	50. methyl isobutyl ketone
13. n-dodecane	32. 1-methyl-2-ethyl benzene	51. methyl chloroform
14. ethylene	33. 1-methyl-3-ethyl benzene	52. acetic acid
15. propylene	34. 1-methyl-4-ethyl benzene	53. ethyl acetate
16. iso-butene	35. 1,3-dimethyl-5-ethyl benzene	
17. 1-butene	36. mesitylene	
18. 2-butene (trans)	37. pseudocumene	
19. 2-butene (cis)	38. carbon dioxide	

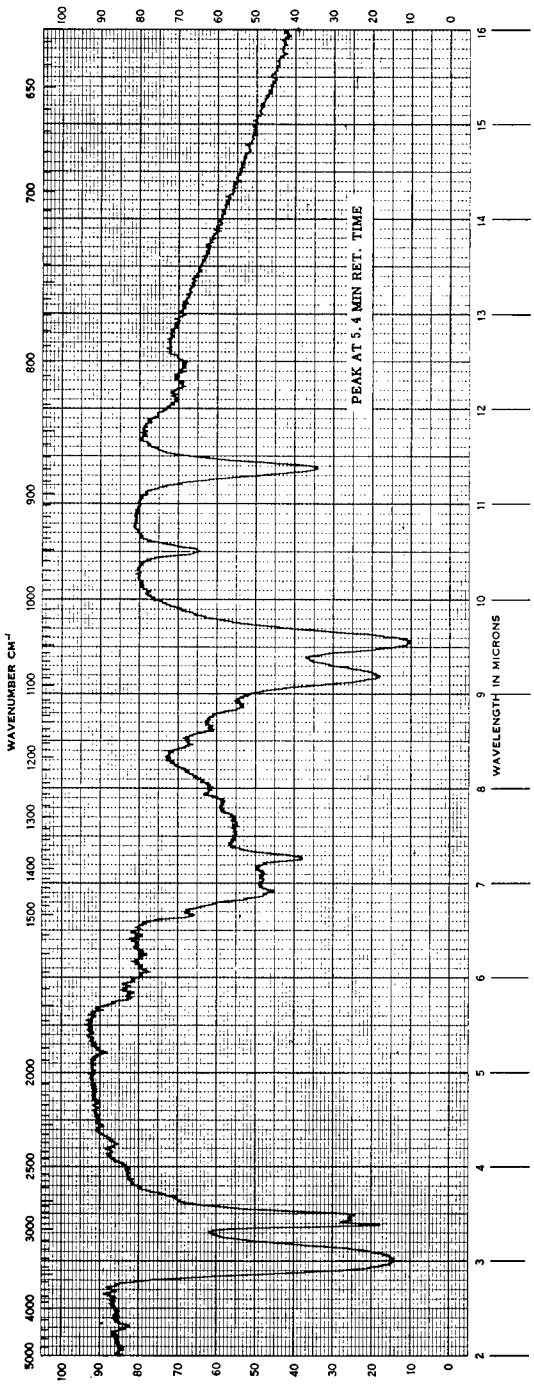

Fig. 7(a) - Infrared spectrum of the peak at 5.4 minutes retention time

UNCLASSIFIED

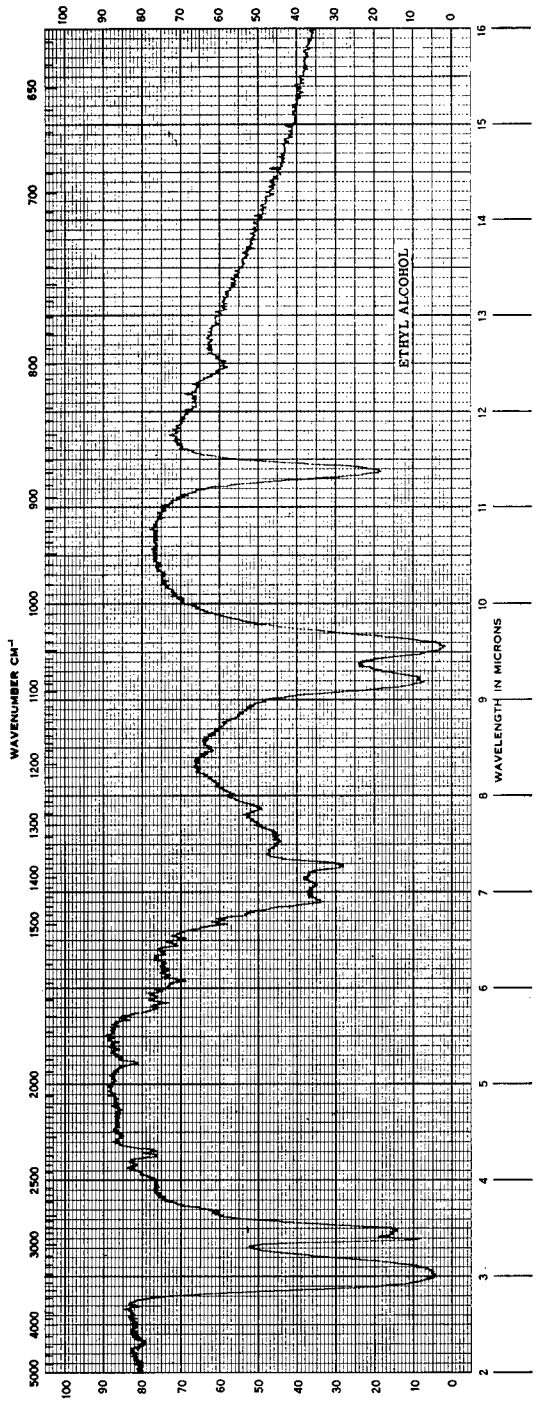

Fig. 7(b) - Infrared spectrum of ethyl alcohol

[redacted]

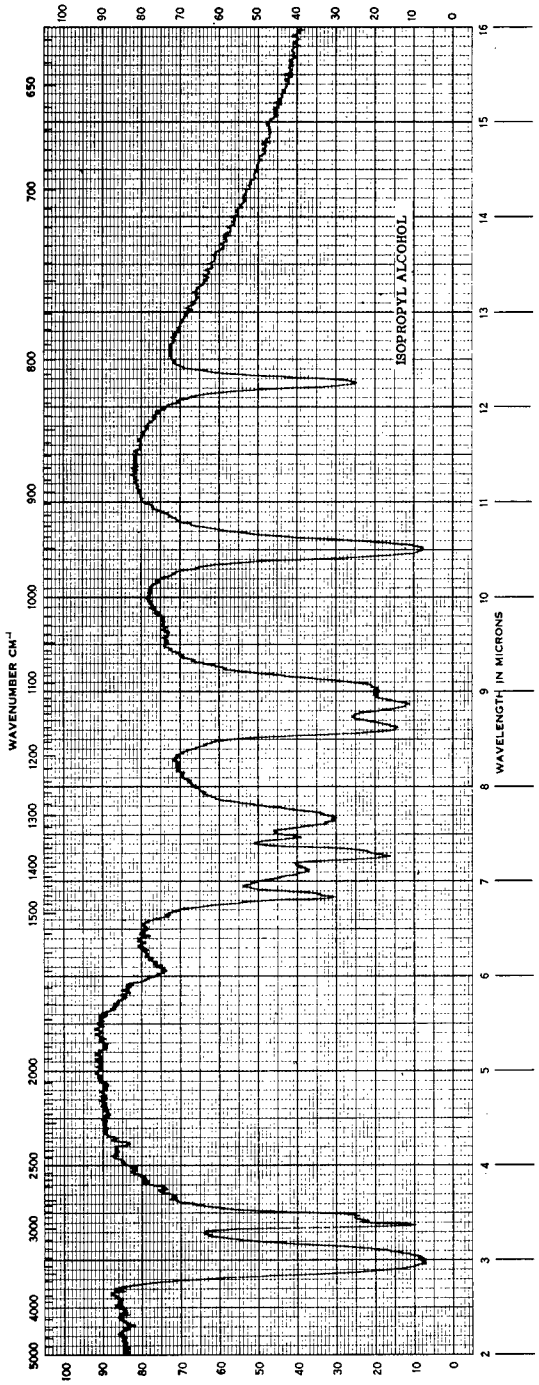

Fig. 7(c) - Infrared spectrum of isopropyl alcohol

[redacted]

UNCLASSIFIED

SUMMARY

The typical nuclear submarine atmosphere is contaminated with an exceptionally complex mixture of organic compounds which originate from cigarette smoke, paint and cleaning solvents, diesel fuel, lubricating oils and a variety of minor sources. No single analytical approach possesses the capability of dealing with such a complicated mixture. However, through the combined use of gas chromatography and infrared spectroscopy, significant progress has been made in identifying a considerable number of trace contaminants.

Perhaps the major limitation in the presently used analytical scheme is the sampling method, namely, adsorption on activated carbon. Lack of data concerning the adsorption-desorption efficiency for the concentration levels normally encountered prevents quantitative analyses at the present time.

Literature Cited

1. Miller, R.R., and Piatt, V. R., "The Present Status of Chemical Research in Atmospheric Purification and Control on Nuclear-Powered Submarines," NRL Report 5465, April 12, 1960

2. Piatt, V.R., and Ramskill, E. A., "Annual Progress Report. The Present Status of Chemical Research in Atmospheric Purification and Control on Nuclear-Powered Submarines," NRL Report 5630, July 14, 1961

[redacted]

RECENT ADVANCES IN GLASS FIBER REINFORCED PLASTIC ROCKET MOTORS

([redacted])

J.A. Kies[1] and Harold Bernstein[2]

The Naval Research Laboratory (Mechanics Division) in anticipation that the performance of the fleet ballistic missile will be materially improved is exploring, on a long range basis, the possibilities of developing new materials and design concepts which go substantially beyond those available now.

Nozzels suitable for flame temperatures above 6300°F and new motor case materials of greater reliability and greater strength/density ratios are being investigated are the possible effects of long term storage and operating environments. These effects include stress corrosion of high strength steels and moisture and craze cracking on glass reinforced plastics. . . . . FBM staff

INTRODUCTION

U. S. Government sponsored and private research and development of fiberglass-plastics for rockets and for other military and space applications is very broad. It is not possible to state here their full extent or scope. The Polaris program of R and D at first glance is aimed at short range answers to assist in setting up materials and process specifications within the next two years. This does however necessitate the investigation of some basic problems of long range interest such as new glasses and finishes, improved resins, mechanisms of failure, ideal winding patterns and contours and many other problems. Our total purpose is far broader than to write specifications for today's use. The real job in coordination is for all of us to learn how to encourage initiative and then make best use of the results of materials research.

COMPARISON OF THE STRENGTH-DENSITY RATIOS AND RELIABILITY OF DIFFERENT MATERIALS FOR SOLID ROCKETS

In todays family of missiles, fiberglass reinforced plastic is the structural material for one of the motor cases in two systems, Minuteman Wing 1 and Polaris A2. Both of these missile systems are expected to become operational within the next few years. In both systems, metal cases are used in the booster stage, but the sustainer stage where the weight-range trade off is significant is constructed of fiberglass. Both the Minuteman and Polaris motor cases are fabricated from E glass and epoxy resin.

Comparison of the structural efficiency of a composite material with a homogeneous material is inexact. An alternate approach is to compare the filament strengths of presently available materials. These are listed below together with the values required to make them equivalent with glass on a strength/density basis:

---

[1]U.S. Naval Research Laboratory, Washington 25, D.C., Mechanics Division.

[2]Special Projects Office, Washington 25, D.C.

[redacted]

UNCLASSIFIED

	Av. Density	Available Strength	Strength Required to Compete with E Glass
E Glass	0.092 lb/in.^{3}	250,000 psi min	
Ti B120 VCA	0.17 lb/in.^{3}	250,000 psi	465,000 psi
Music Wire	0.28 lb/in.^{3}	600,000 psi	820,000 psi

The homogeneous metals appear in a more favorable light if composite strengths are considered, as follows:

	Av. Density	Stress/Strength
E Glass-Epoxy	0.072 lbs/in.^{3}	60,000 psi (Polaris A2 second stage proof)
Titanium B120 VCA	0.17	170,000 psi Yield Strength
Tricent Steel	0.28	240,000 psi Yield Strength
Nickel (25%) Iron alloy	0.30	260,000 psi Yield Strength

All of the metals listed appear to be competitive with the fiberglass reinforced plastic, assuming that they could be reliably proof tested to yield strength level. However, the titanium and steel alloys are very brittle at these strength levels. Recent tests on the nickel iron alloy have demonstrated excellent toughness at the high strength level, but this alloy is still in the developmental stage. The technology of high strength steel pressure vessels has progressed to the point where high reliability can be obtained in motor cases operating at the 200,000 psi level (strength-weight ratio 0.7×10^6). A large amount of research and development appears necessary in order to achieve reliability with steel motor cases at the 240,000 psi strength level. In two programs with this objective, carried out by reputable contractors for advanced Polaris second stage motor cases, one failed dismally, and the second was only partially successful. In addition, the metals fabrication technology requires extensive tools and fixtures, long lead times and is relatively inflexible to design changes. All of these considerations plus the resultant cost factor favor the fiberglass-plastic motor case over the steel motor case.

It may help to compare actual weights, although the picture is clouded by non-uniform designs. An advanced Polaris first stage motor, 14 feet long × 54 inches in diameter, fabricated from steel, weighed 1230 lbs. Advanced first stage motor cases fabricated from fiberglass reinforced plastic weighing approximately 800 lbs are presently available. With an equivalent design for the steel case, it would be theoretically possible to thin the chamber walls and reduce the weight to 1000 lbs. However, the fabrication problems would increase by an order of magnitude with thinner structural components.

The factors which demonstrate reliability in a motor case are consistent performance in static and flight tests and retention of properties after extensive storage time and exposure to moisture and other environmental contaminants. In the early part of the Polaris A2 second stage fiberglass motor case program, failures in hydrotest were numerous. Approximately one out of three cases failed, for a variety of reasons most of which stemmed from fabrication problems. Once these problems were overcome, the failure rate was substantially reduced. In the first half of 1961, all hydrostatic tests of A2 second stage motor cases were successful.

The performance of fiberglass cases in flight test has been highly satisfactory to date. In twelve down range flights of the A2 missile, all objectives have been achieved. With regard to problems of storage life, controlled surveillance programs are underway.

However, observations from numerous sources indicate that fiberglass reinforced plastic has good durability. For example, channel marker buoys and pontoons for marine floats showed no signs of degradation after immersion in salt water for 3-1/2 years. Test sections of fiberglass have been exposed to outdoor (California) environments for five years with no loss in strength. Rocket motors have been stored outdoors in the northeast section of the United States for one year periods prior to successful firing tests.

Under sensibly statis conditions, fiberglass reinforced plastic, using one of the commercial epoxy resins will retain about 75% of its strength up to 300°F, above which temperature the strength fall off rapidly. The fiberglass motor case gets heat from two sources, the burning fuel and aerodynamic friction. Of course, internal temperatures are so high that internal insulation is needed to shield the casing. Temperatures reached on the exterior by aerodynamic heating are more moderate and are effective for very brief intervals. However, some exterior insulation may be needed. Because of the weight penalty, it is necessary to minimize external insulation and if possible eliminate it. The development of resins retaining full strength to 500°F would be helpful toward reaching the latter goal.

The Polaris A2 fiberglass motor case is pressurized at proof to a composite hoop stress of 60,000 psi. The corresponding filament stress is 135,000 psi, which when compared with present available strength of glass indicates substantial growth potential. In addition, E glass with an improved finish is available now in limited quantities and higher strength compositions are under development. The experimental models of the A3 motor case first and second stages are both fabricated from fiberglass and attain a composite hoop stress of 80,000 psi at proof pressure. The goal of 100,000 psi appears attainable in the not too distant future.

EFFECTS OF INHERENT FLAWS

Irregularities in glass and Resin

The stated goal, a composite strength of 100,000 psi, does not include a statement of safety factor, but a high reliability say 99+% is applied. The actual available burst strengths are a matter of guess and extrapolation from small statistical samples. Variability in materials, processing, and the effects of built-in flaws are still not adequately known. A rather large number of such defects were mentioned in previous papers (Refs. 1, 2, and 3). Satisfactory measurement of the effects of different flaws on strength of a pressure bottle usually requires that we have only one kind of flaw at a time to measure or at least that the flaw such as a snarled or knotted group of rovings embedded in the finished rocket will be the worst flaw in the structure under test. For satisfying the immediate demands on strength our experiments with knots in hoops indicates that a single such knot will not interfere with the 100,000 psi goal but that two or more knots spaced less than 1.2 inch apart will reduce the strength well below that figure. A recent full scale verification of this test result was obtained by accident. It happened that a new operator, not having attended the Palo Alto Conference in June 1961, tied seven knots about 1-1/4 inches apart in order to connect new spools during the winding of a first stage A3. The chamber burst during hydrotest with the fracture originating at the location of the knots. Other kinds of defects too numerous to mention here are being investigated but only in a preliminary or exploratory fashion. It is almost impossible to characterize in a precise scientific fashion all of the possible irregularities in fiberglass-plastic so that the decision of what constitutes a defect and what is tolerable will require a great deal of future experience.

UNCLASSIFIED

DEBONDING FRACTURES

A considerable number of pressure test failures in the past have been associated with debonding between fiberglass and metal bosses or cluster plates. This was perhaps present during processing. To a large extent this difficulty has been eliminated empirically by suitable joint modifications which cut down on stress concentration. For future optimization of strength-weight in the structure, a rather sophisticated study of bonded joints is in progress. Detailed stress analysis of cracks in the form of partial debonds are under development but not yet achieved. For immediate use in evaluating the fracture resistance of bonds between laminae having widely different elastic coefficients, we have available a simple fracture mechanics method. The principle has been described elsewhere (Ref. 4). It essentially consists of utilizing the concept of elastic strain energy release rate as given by

$$\mathcal{G}_c = \frac{F^2}{2} \frac{d\left(\frac{1}{M}\right)}{dA}$$

where F is the load, 1/M is the elastic compliance of the specimen containing a crack, and A is the fractured area. This method is not restricted to a single pair of loading grips and it is, in principle at least, capable of dealing with any specimen no matter how complicated in geometry. No theoretical stress analysis is needed for this procedure.

The results of this research are intended to provide scientific evaluations and guides to optimizing different joint parameters such as thickness, elastic coefficients in different layers, geometry or design, and fracture toughness. Such studies are intended also to predict critical allowable flaw sizes and shapes and thus guide the requirements for nondestructive test standards. This latter is a proper objective of all fracture mechanics research. This method allows any combination of shear and tension to be applied to the bond in the specimen. The most important requirement of the experiment is to obtain by calibration the values of 1/M vs slot size in specimens just like the ones to be fractured. An equation 1/M vs x(x- slot size) consisting of a power series is written to fit the calibration data. This equation is then differentiated to give d(1/M)/dA for use in the fracture experiment.

VULNERABILITY TO MECHANICAL DAMAGE

Materials Evaluation

For military applications this topic is of greater importance than in ordinary civilian or commercial life. Design and manufacturing people can in theory refine fiberglass rocket cases to stand composite stresses of even 200,000 psi in laboratory tests. Such strengths remain available only if wartime field conditions including exposure, handling, and accident resemble the laboratory environment and test conditions. Here we have made some progress on flaw evaluation, although much more remains to be done.

One kind of rupture failure rather commonly experienced, but not the only one, consists of an unwrapping effect in the hoop, wound outer layers of a rocket motor case while under internal pressure. Figure 1 is a typical photograph of such a failure. It is hypothesized that this and other similar failures could start from a small dent or scratch or manufacturing defect which in effect severs a bundle of filaments. A shearing stress then develops between this bundle and its surroundings and when the resin cracks or debonds along this boundary the bundle splits away. The energy for the process can come from the strain energy in the bundle. Figure 2 shows schematically how a rectangular bundle in the process of unwinding gives up its strain energy. We shall refer to the formulas later.

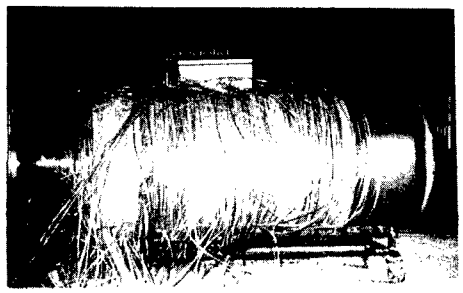

Fig. 1 - Photograph of failure in hoop windings

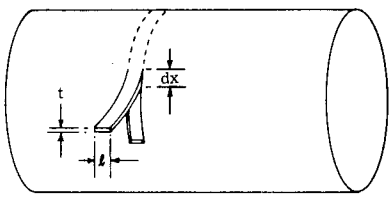

For initiation of peeling of hoop windings from outside.

$$-\frac{\partial E_s}{\partial A} = \frac{dW}{dA} = \frac{\partial}{\partial A}\left[\frac{\sigma^2}{2E}\ell t\, dx\right]$$

$$dA = (\ell + 2t)\, dx$$

$$\mathcal{G}_c = \frac{dW}{dA} = \frac{\ell t}{\ell + 2t}\,\frac{\sigma^2}{2E}$$

t = thickness of strip
ℓ = width of strip
E = Young's modulus
σ = hoop stress

$\frac{dW}{dA}$ = work per unit area for the stripping

Fig. 2 - A rectangular strip of hoop windings splitting away

Tests were made on 18 inch diameter, one inch wide, hoops with edge cuts and with outer surface cuts of known size and configurations. Photographs of representative notches are given in Figs. 3 and 4. The hoops were pulled in tension and the load recorded when the split became easily visible (at about 0.25 inch length). It was assumed that all of the strain energy released from the bundle was used in propagating the split. On this basis for the edge notches the condition of failure is

$$E\,\frac{dW}{dA} = \frac{\sigma^2 \ell}{2} \tag{1}$$

where E is Young's modulus for the composite, dW/dA is the work per unit area for fracture propagation, assumed constant, σ = the composite hoop stress, and ℓ is the depth of the edge notch. In the experiment it is not necessary to know E since the combination E dw/dA is the materials parameter controlling the relation between stress and notch depth. The formulas cannot be expected to work well for notch area in excess of half the specimen cross section.

UNCLASSIFIED

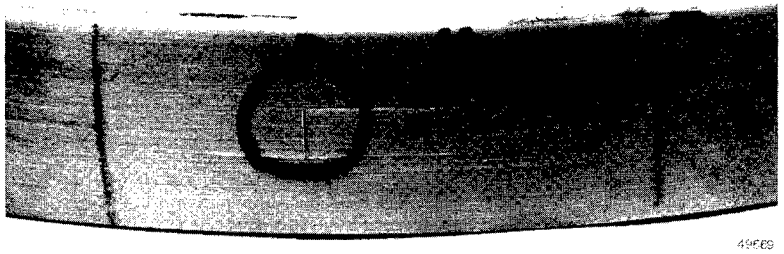

Fig. 3 - Photo of edge notch in a test ring

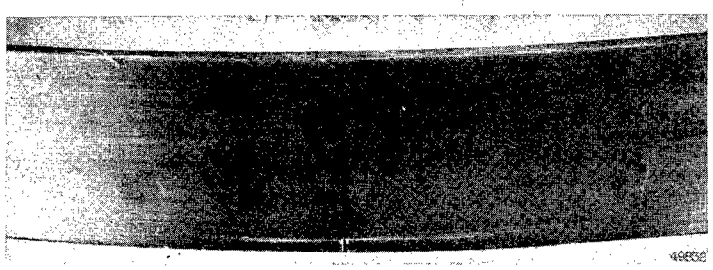

Fig. 4 - Photo of a surface notch in a test ring

Similarly for transverse surface cuts in the rings,

$$E \frac{dW}{dA} = \frac{\sigma^2}{2} \frac{c}{S} \tag{2}$$

where c is the cross-sectional area of the cut and S is the submerged perimeter of the cut.

Figures 5 and 6 show data from these ring tests in which

$$K_c^2 = E \frac{dW}{dA} \tag{3}$$

was determined to be 31×10^6 lb^2/in^3 for the combination of E glass in Epon 826. The glass was 80% by weight. Note that the data fit reasonably well on the theoretical curve fitted to one point on the graph.

It is suggested that this method of testing is simple, cheap, and useful for indicating the resistance of any hoop wound layers to damage possibly leading to unwinding failure. The effects (perhaps beneficial), of increased winding pitch or cross over, and of improved resin ductility, crazing, and shrinkage stresses are a few parameters that can be measured in this way.

In estimating the effects on strength of mechanical damage to full scale motor cases the forgoing hoop formulas are not adequate. Accordingly in studying failure by the unwinding of hoop layers such as shown in Fig. 1, we make the same basic assumption that was made for the ring splitting test, i.e., all of the released strain energy goes into crack propagation. If we can derive an equation of a useful functional form it will assist in assigning constants characterizing the quality or vulnerability of the motor case.

[redacted]

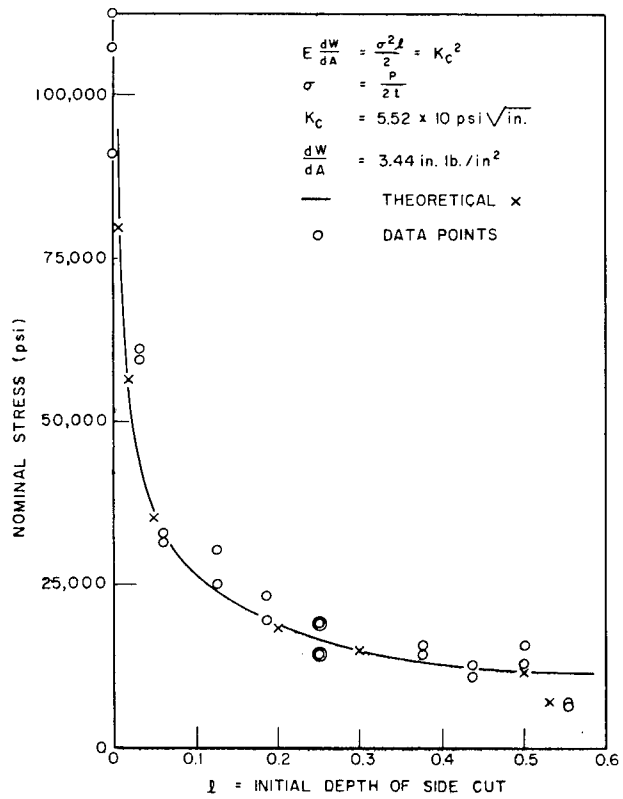

Fig. 5 - Test data and formulas for edge notch rings

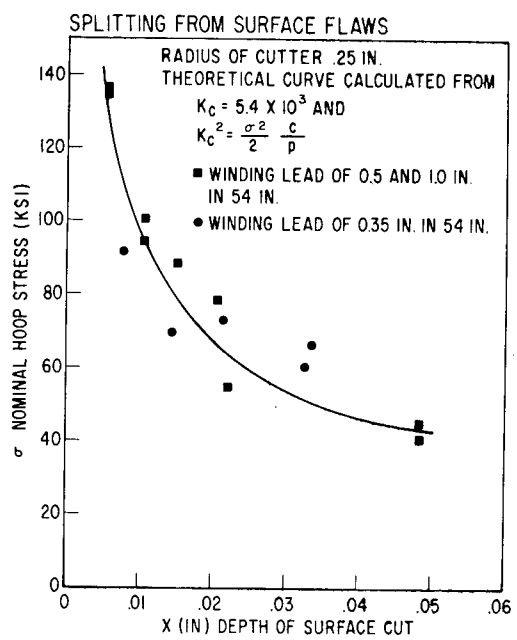

Fig. 6 - Test data and formulas for surface notched rings

UNCLASSIFIED

Prediction of Failure Due to Mechanical Damage in the Outer Hoop Windings to a Fiberglass Plastic Pressure Vessel

Let σ_h = the mass hoop stress in the outer hoop wound layer

σ_ℓ = the mass longitudinal stress in the outer hoop wound layer

σ_1 = mass hoop stress in the entire wall

σ_2 = mass longitudinal stress in the entire wall.

Consider a scratch or gouge which cuts fibers over an apparent or surface length ℓ and to some depth b. Without specifying the shape of the gouge we can say that the submerged part of the perimeter of the broken bundle is S.

In response to the hoop stress σ_h we have a driving force K_h and separately a K_ℓ in response to the longitudinal stress σ_ℓ. Let $\mathcal{E}$ = elastic energy. Let $-d\mathcal{E}_h$ = a small release of energy due to stress relieval in a tongue of material unwinding and splitting away in the hoop direction. Let $-d\mathcal{E}_\ell$ be a small release of energy due to the longitudinal stress acting normal to the split, $-d\mathcal{E}_\ell$ is the same as that ordinarily considered in the Griffith formula.

Assuming plane stress and no distortion

$$\left.\begin{aligned}
\epsilon_h &= \epsilon_1 = \frac{1}{E_1}(\sigma_1 - \nu_2\sigma_2)\\
\epsilon_\ell &= \epsilon_2 = \frac{1}{E_2}(\sigma_2 - \nu_1\sigma_1)\\
\sigma_h &= E_h\,\epsilon_h = \frac{E_h}{E_1}(\sigma_1 - \nu_2\sigma_2)\\
\sigma_\ell &= E_\ell\,\epsilon_\ell = \frac{E_\ell}{E_2}(\sigma_2 - \nu_1\sigma_1)
\end{aligned}\right\} \tag{4}$$

$\sigma_1 = \frac{PR}{T}$ $\quad \sigma_2 = \frac{PR}{2T}$ where P = internal pressure

R = radius of the cylinder and T is the wall thickness.

Then

$$\left.\begin{aligned}
\sigma_h &= \frac{E_h}{E_1}\frac{PR}{T}\left(1 - \frac{\nu_2}{2}\right)\\
\sigma_\ell &= \frac{E_\ell}{E_2}\frac{PR}{T}\left(\frac{1}{2} - \nu_1\right)
\end{aligned}\right\} \tag{5}$$

The energy per unit volume assuming $\tau_{xy} = 0$ is

$$\mathcal{E}_h = \frac{1}{2}\left[\frac{\sigma_h^2}{E_h} + \frac{\sigma_\ell^2}{E_\ell}\right] - \frac{\sqrt{\nu_h}}{\sqrt{E_h}}\,\sigma_h \cdot \frac{\sqrt{\nu_\ell\,\sigma_\ell}}{\sqrt{E_\ell}} \tag{6}$$

Phillip Mast (Ref. 5) has computed values of E_ℓ, E_h, E_1, E_2, ν_ℓ, ν_h, ν_1, and ν_2 for the special case of n longitudinal windings and 2n hoop windings assuming 20 percent resin by volume having an intrinsic $E_p = 5 \times 10^5$ psi and $\nu_p = 0.4$. He also assumed an intrinsic $E_g = 10.5 \times 10^6$ psi and $\nu_g = 0.25$ for glass. The computed values are on the following page.

[redacted]

E_h = 8.1×10^6 psi = Young's modulus in the hoopwise direction for the outer hoop wound layer.

E_ℓ = 2.4×10^6 psi in the longitudinal direction i.e., transverse to the filaments in the outer hoop wound layer.

E_1 = 6.1×10^6 psi in the hoop direction for the composite.

E_2 = 4.1×10^6 psi in the longitudinal direction for the composite.

ν_h = Poisson's ratio in the outer hoop windings for stress applied in the hoop direction = 0.284.

ν_ℓ = 0.056 in the outer hoop wound layer.

ν_1 = 0.21 = Poisson's ratio for hoop stress in the composite.

ν_2 = 0.065 for longitudinal stress in the composite.

For convenience in solving crack propagation problems for this case and for the unwinding type of failure we now express E_h and E_ℓ in terms of E_1

$$E_h = \frac{8.1}{6.1} E_1 \cong 1.33\, E_1$$

$$E_\ell = \frac{2.4}{6.1} E_1 \cong 0.394\, E_1 \qquad \frac{E_\ell}{E_2} = \frac{2.4}{4.1} = 0.586$$

and

$$\nu_\ell = \frac{0.056}{0.21} \nu_1 = 0.267\, \nu_1$$

$$\nu_h = \frac{0.284}{0.21} = 1.35\, \nu_1.$$

Then remembering that $\sigma_2 = \frac{\sigma_1}{2}$,

$$\sigma_h = 1.29\, \sigma_1$$

$$\sigma = 0.170\, \sigma_1$$

in the outer hoop wound layer.

Using numerical relationships above we can simplify equation (6) to

$$\mathcal{E}_h = \frac{\sigma_1^2}{2E_1}(1.142). \tag{7}$$

For a flaw such as described in Figs. 7 and 8 in a motor case as assumed:

$$\frac{-d\,\mathcal{E}_h}{dA} = \frac{\sigma_1^2}{2E_1} \cdot \frac{c}{s} \quad \text{where} \quad \sigma_1 = \frac{PR}{T} \tag{8}$$

P = pressure in the motor case, R is the radius, and T is the wall thickness in the cylindrical part.

UNCLASSIFIED

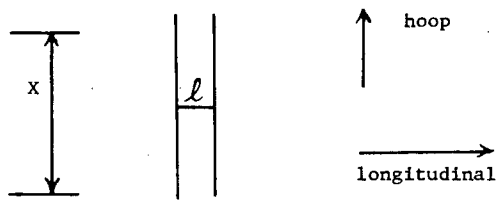

X is the total length of the split away part.

Fig. 7 - Surface diagram of splitting from a surface scratch

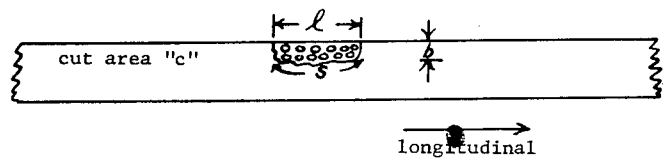

Fig. 8 - Section diagram of splitting from a surface scratch

For convenience in referring to notched ring tests in which K_{hc} (Irwin toughness parameter) is determined using only hoop windings

$K_{hc}^2 = -E_h \frac{d\mathcal{E}_h}{dA} = 31.9 \times 10^6$ from our tests. Subscript c indicates a critical value of K_h.

For the motor case using $E_h = 1.33\ E_1$

$$\frac{-d\mathcal{E}_h}{dA} = \frac{\sigma_1^2\ (1.33)}{2E_h}\ \frac{c}{S} \tag{9}$$

$$K_h^2 = 0.67\ \sigma_1^2\ \frac{c}{S} = 0.67\left(\frac{PR}{T}\right)^2\ \frac{c}{S}\ .$$

According to Irwin (Ref. 6) the Griffith energy release rate depends only on the component of stress normal to the crack (which in this case propagates in the hoop direction).

$$\therefore\quad \frac{-d\mathcal{E}_\ell}{dA} = \frac{\pi\sigma_\ell^2\ bx}{2E_\ell S} \tag{10}$$

and

$$K_\ell^2 = \frac{\pi\sigma_\ell^2\ bx}{2S}\ . \tag{11}$$

Since

$$\sigma_\ell = 0.170\ \sigma_1 = 0.170\ \frac{PR}{T}$$

$$K_\ell^2 = 0.0453\ \left(\frac{PR}{T}\right)^2\ \frac{bx}{S}\ . \tag{12}$$

The total driving force in terms of K_h^2 and k^2 is

$$K^2 = K_h^2 + K_\ell^2 \tag{13}$$

[redacted]

or

$$K^2 = \left(\frac{PR}{T}\right)^2 \left[0.67\,\frac{c}{S} + 0.0453\,\frac{bx}{S}\right]. \tag{14}$$

K^2 is always positive increasing with x. Therefore instability is permanent once achieved under constant P.

It should be kept in mind that the numerical coefficients of c/s and bx/s are subject to revision based on other known ratios of elastic constants for real motor cases. It's believed that the above functional form is essentially correct and that it is potentially useful in discussing vulnerability.

Example:

Calculation of unstable scratch depth for x = 0. Assume PR/T = 80,000 psi.

$$K_c^2 \doteq K_{hc}^2 = \left(\frac{PR}{T}\right)^2 (0.67)\,\frac{c}{S}$$

$$K_h^2 \text{ critical} = 31 \cdot 10^6 \text{ lb}^2/\text{in.}^3 \text{ for tests.}$$

$31 \cdot 10^6 = (80)^2 \cdot 10^6\,(0.67)b$ where b is the scratch depth short with respect to the scratch length (Ref. 3).

$$b = \frac{31}{(80)^2\,(0.67)} \doteq \frac{31.00}{4300} = 0.007 \text{ inch.}$$

This is intermediate value between two other values, 0.004 inch and 0.013 inch, obtained by going to opposite extremes in probable values of the ratios of elastic constants.

To many engineers accustomed to estimating remaining strength on the basis of the net average stress on the holding area in ductile materials, such a small critical size prediction (.007 inch deep) may seem unreasonably pessimistic. Fracture Mechanics teaches that fracture propagation from small flaws in brittle materials is not a matter of net section stress entirely but is instead a function of the flaw size and stress even though flaw is too small to appreciably alter the average net section stress. Our results on notched rings bear this out.

NONDESTRUCTIVE TESTING

At present we already have at hand many instruments such as X-ray, ultrasonic, corona discharge and penetrants to detect far more kinds of irregularities and presumable defects in fiberglass rockets than we know how to correlate with strength and reliability. We cannot begin to mention all of the recent developments in this area but great advances have been made in the joint Polaris, Minuteman, and Pershing working panel under the Chairmanship of CDR. R. Smiley.

One illustrative example in which NRL is active consists of recent work in the art of nondestructive detection and measurement of moisture in the motor cases as they proceed through processing, storage, and exposures at sea. There is ample room for debate as to whether moisture pick up is bad or not. Without question it has been shown that glass fibers freshly drawn from the bushing degrade in strength on contact with moisture. It's not easy to show that moist air degrades rocket motor cases. Since

UNCLASSIFIED

crazing in the resin is prevalent after hydrotest it is conceivable that moisture can enter especially into craze cracks and degrade the material. Two new instruments have been developed for the Navy, one by Mr. John Abel of NRL (Ref. 8) and another by Prof. Outwater and his staff at the University of Vermont (Ref. 9). The first of these measures the Q of a circuit which includes a probe held against the motor case. The second measures Q and the dielectric constant (real part) with a similar probe. It is not suitable to give detailed results at this time because Mr. Abel and Prof. Outwater will eventually publish their own findings. Contaminants other than moisture can affect the readings and hence the interpretation. The purpose here is merely to call attention to one of many controversial questions regarding the use and interpretation of nondestructive test findings.

REFERENCES

1. Bernstein, H., and Kies, J.A., "The Fiberglass Motor Case in the Polaris Program," Society of Aerospace Material and Process Engineers Filament Winding Symposium, March 28-30, 1961, Pasadena, California. Naval Research Laboratory Report No. 5650 dated September 19, 1961.

2. Hart, S.D., and Kies, J.A., "Some Problems in the Detection and Evaluation of Flaws in Glass Fiber Motor Cases," Missiles and Rockets Symposium, Bureau of Naval Weapons at U. S. Naval Ammunition Depot, Concord, California, April 18-21, 1961

3. Hendron, J., "Nondestructive Testing Status of Glass Filament Wound Solid Rocket Chambers," July 1961, Aerojet-General Report.

4. Irwin, G.R., Kies, J.A., and Smith, H.L., "Fracture Strengths Relative to Onset and Arrest of Crack Propagation," NRL Report 5222, November 20, 1958, and Proc. ASTM Vol. 58 (1958)

5. Mast, P., Unpublished communication

6. Irwin, G.R., Unpublished communication

7. Ewing, H.O., and Kies, J.A., NRL Progress Report, October 1961

8. Abel, J., "Nondestructive Testing of Glass Epoxy Polaris Motor Cases," Presented at the 18th POLARIS/MINUTEMAN/PERSHING Nondestructive Test Committee Meeting, Salt Lake City, Utah, 2-3 August 1961. Not yet available for public distribution.

9. Gagne, G.A., and Outwater, J.O., "A Portable Electronic Moisture Detector for Reinforced Plastics," University of Vermont Report, Oct. 15, 1961

[redacted]

IN SITU HALL EFFECT MEASUREMENTS ON THIN GERMANIUM FILMS

(Unclassified)

J. E. Davey and M. D. Montgomery

The Naval Research Laboratory (Electronics Division) is currently investigating advanced techniques for vacuum deposition of germanium films on amorphous substrates. Preliminary success in the deposition of textured germanium films on fused quartz substrates and single crystal films has led to the initiation of device-oriented experiments designed to yield multilayer geometrics in which the possibility of p-n junction action is maximized.

. . . . . FBM staff

INTRODUCTION

Semiconductors, in thin film form, are presently of great interest from the point of view of their ultimate usage in microminiaturized devices. However, many of the basic properties of these films in both polycrystalline and monocrystalline form, are still unknown. In this report we will describe an experimental program on germanium films which is concerned with a determination of their electrical properties. Specifically we are concerned with determining the effect of thickness, source impurities, ambient impurities, and surface effects on the impurity type, concentration and the band picture for germanium films.

Since resistance measurements on germanium films deposited in commercial evaporating systems at 10^{-5} mm, show a marked increase upon exposure to gas or air, it is to be expected that the interpretation of the electrical properties of the films will be seriously affected by the ambient in which they are made and measured. (This is not unexpected, per se, due to the known great surface sensitivity of Ge.) Thus in this work we are attempting to optimize the ambient control and impurity control by making all measurements, in situ, in a ultra-high vacuum system, which also allows gas filling. The measurements are first being performed on polycrystalline films since it has yet to be shown that crystallinity or lack thereof is the determining factor in the impurity conduction mechanism. Thus by starting with polycrystalline films, a change of crystalline order may be caused first by annealing, second by hot deposition and annealing and finally by a vacuum epitaxy on signal crystal surfaces.

EXPERIMENTAL

The experimental tube is shown in Fig. 1. The evaporation system in this tube consists of a hollow tungsten anode which is bombarded by electrons released from a hot tungsten filament surrounding the anode. The shielding and slit system surrounding the filament allows no evaporated tungsten from the filament to be seen by the substrate. The germanium is loaded into the gun by means of the side arm and spout. Before loading the gun system is vigorously outgassed at 2000°C under optimum high vacuum conditions. When the Ge is loaded into the gun, the shutter section of the ferris wheel is brought over the evaporation port, the gun is then stabilized at the evaporation temperature. After stable evaporating conditions prevail, the ferris wheel is turned until the first glass monitor is in the evaporation port. (Since the relative distances between evaporator, glass monitor, and substrate, are known, by measuring the thickness on any monitor, for a given evaporation

[redacted]

UNCLASSIFIED

time, the thickness at the substrate can be thereby calculated. The thickness measurements on the monitors can not be made until the termination of the experiments, and the tube is cut open.) After a measurable film thickness has been deposited on the monitor, the ferris wheel is turned to an open section in the wheel, and the substrate is turned normal to the evaporation beam. (All movable parts have a small covar tab welded to them which may be manipulated from outside the tube by small permanent magnets. All parts pivot around a central tungsten aligning rod which is shown in Fig. 1.) During the evaporation, the substrate is heated optically to approximately 300°C by focusing two Sylvania "tru-flector" bulbs on the back of the substrate. Hot deposition at this temperature guarantees that the deposit will be crystalline and between the two strong texture states for germanium films (1). Figure 2 shows the substrate and mask. The electrical system in the substrate was made by sealing five tungsten rods between two Nonex plates such that right angle bends in the tungsten rods protruded through the plates in the configuration shown in Fig. 2. The whole mass was sintered, annealed, cooled, and polished to within 200A flatness. The substrate was then carefully cleaned, mounted in a commercial vacuum evaporator and rhodium was hot-vacuum deposited at 600°C in the Hall configuration shown in Fig. 2. The Ta mask is then attached and substrate with mask loaded on the pivot system in the ultra high vacuum tube. The Ta mask allows a rectangular deposit of Ge to just cover the ends of the rhodium Hall probe system. Connections between the press and the substrate are made by welding flexible tungsten leads which are insulated with glass beads.

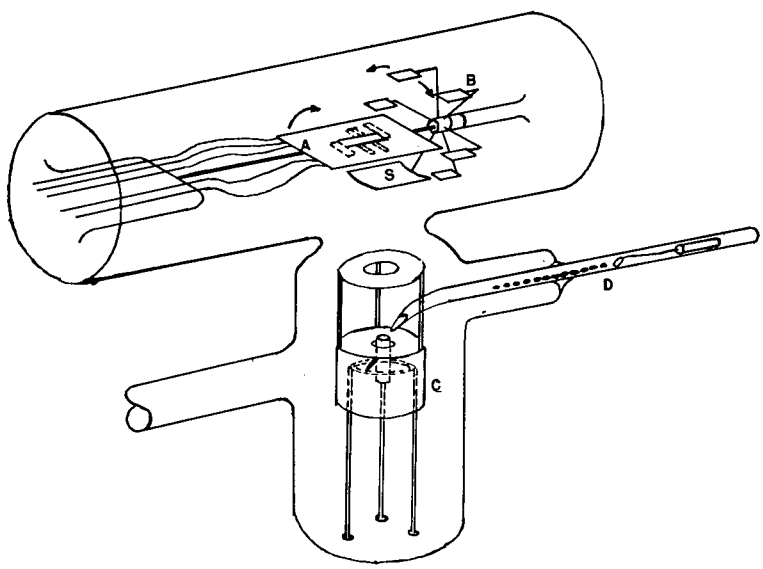

Fig. 1 - (A) Hall sample under slotted Ta defining mask. Contacts are made to rhodium deposited on tungsten wire sealed into glass substrate. The tungsten wires protrude through the glass surface, at right angles, and are polished optically flat with the receiver surface. Flexible, glass insulated electrical leads go between the Hall sample and the press. (B) A ferris wheel arrangement of glass slices plus a Ta shutter S. The thickness of the film on the Hall sample is monitored by the thickness on these slices. (C) Electron gun structure consisting of a curcular W filament as electron source, a recessed W cylinder as anode, (the charge of Ge being dropped into the recess for evaporation), and a surrounding heat shield and evaporation slit system. (D) The side arm containing a supply of Ge particles for loading separately into the electron gun. The train of particles is moved by the magnetic plunger shown in the arm.

[redacted]

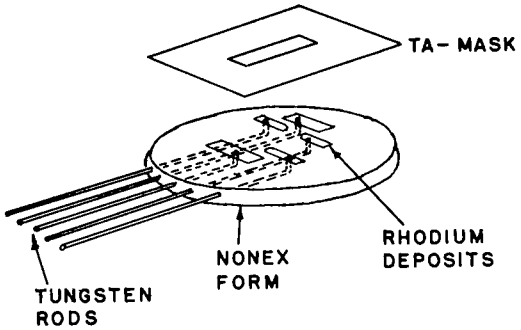

Fig. 2 - Substrate and mask

The gas filling ultra-high vacuum system is shown in block diagram in Fig. 3. The processing procedure involved in these experiments was as follows. All parts are cleaned rigorously and etched where possible. The source Ge is newly cleaved 30 ohm-cm particles which are loaded after the tube and all parts are mounted on the vacuum system. All glass blowing operations and sealing was done under continual Argon flush and the system leak checked with a well trapped helium leak detector. The tight system was evacuated to approximately 10^{-7} mm and cyclic processing begun. That is, the system was baked at 425°C, cooled and then all metal parts outgassed. This procedure was repeated for better than 30 hours baking time until the pressure was approximately 10^{-9} mm at the Alpert gauge on the tube. The experimental tube was then closed off from the vacuum system by bakeable valve #1 and the tube was pumped by the Vac-Ion and Alpert gauge alone to about 10^{-10} mm. The electron gun evaporator was again outgassed, loaded with Ge and the evaporation series, which have been described above, were started.

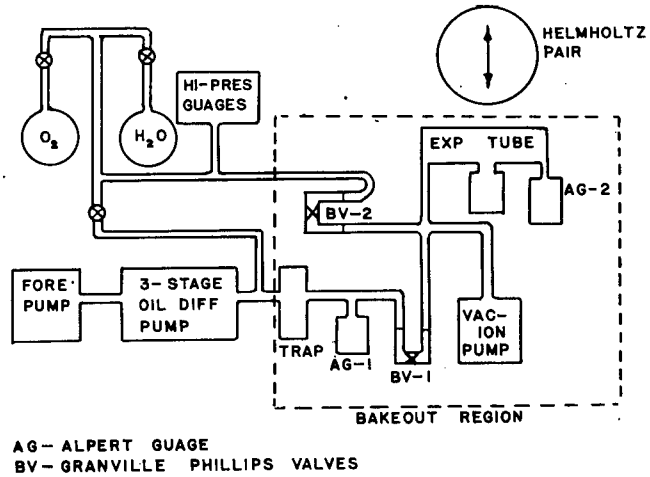

Fig. 3 - Ultra-high vacuum – gas filling system

Immediately subsequent to an evaporation onto the substrate, the substrate is turned normal to its evaporation position, and Helmholtz coils lowered over the tube and Hall and resistivity measurements made. The whole evaporation cycle is repeated with the second monitor, the third and so on, until all thickness monitors are used. The maximum film thickness so obtained, in the present series, was 16000°A. Depending on the specific type of information sought, at any particular thickness, temperature variation of resistivity could be made, and also the effect of gaseous ambients on resistivity, mobility and carrier

UNCLASSIFIED

sign. However, if gases are introduced at intermediate thicknesses, complete regeneration may not be affected by annealing alone (due to the low annealing point of the substrate) such that some degree of uncertainity would be inherent in the results of further evaporations. Thus in the present work, no gases were introduced until after the last evaporation. This of course decreases somewhat, the sensitivities to surface effects since the thickness is rather large.

RESULTS

Measurements of the impurity concentration and mobility as determined from the Hall measurements are shown in Fig. 4 as a function of thickness. The resistivity evaluated from the Hall data is shown in Fig. 5 with a few calculated points from Fig. 4 to show the shape of the curve. Some general remarks may be made about the expected behavior of μ and p for thin films. First, the effect of the double scattering surfaces should decrease the mobility as the films become thin. However, if the particle size becomes large, the measured mobility should approach bulk values. In these experiments, an attempt was made to hold particle size constant by hot deposition at one temperature. Seemingly then the mobility should level off beyond about 1000 to 5000A at which thickness X-ray measurements (1) have shown optimum particle size to be extant. Since the mobility apparently continues to change with thickness, it is considered that there is probably a continued slow growth of particles and necks which is beyond the detection range of X-ray half-width measurements. If surface states and associated space charge effects were not important in going from the very thin to thick films, we would not expect the value of p to change with thickness. However, if surface states are important and their density is N_s/t where N_s is the surface density and t is the effective space charge layer, then for these measurements an effective maximum would be

$$P_{max} = \frac{10^{14}\ \mathrm{cm}^{-2}}{10^{-5}\ \mathrm{cm}} = 10^{19}/\mathrm{cm}^3$$

this considers the screening length to be greated than the film thickness at 1000A, the maximum surface density of approximately $10^{14}/\mathrm{cm}^2$ to be occupied and the states to be acceptor type. Now if the 30 ohm-cm evaporated material were to be deposited as 30 ohm-cm material for very thick layers, then one would expect the p value to fall off toward $10^{14}/\mathrm{cm}^3$ with increasing thickness and/or particle size. The concentration evaluation in Fig. 4 shows a continual but slow decrease in p beyond the expected optimum particle size. That is, the p decrease also seems to indicate a changing particle size and remanence of still measurable surface effects.

In an attempt to qualify the state of the surface the tube was gas filled with highly purified H_2O, the surface "regenerated" after pump down, by heating at the substrate temperature used during deposition, and then filled with pure oxygen and the whole cycle repeated. Some of the results are shown in Fig. 6. The effect of both H_2O and O_2, is to decrease the carrier concentration and the mobility. It is concluded that in these particular experiments both gases have acted like suppliers of donor states to the surface and that the films are still surface sensitive up to 16000A and very strongly p-type.

CONCLUSIONS AND RECOMMENDATIONS

Even though the manufacture and measurement of the Ge films, in the present work, was done, in situ, under high vacuum conditions the Hall measurements indicated p-type conduction for all thickness and under all ambients conditions. This p-character has also been observed by us and others (2,3,4) when the films are manufactured at higher pressures (approximately 10^{-5} mm) and the measurements made in air. However, it is patent from the present work with oxygen and H_2O ambients, that the films are surface sensitive and that for unambiguous interpretation of behavior of these films, ultra high vacuum work must be continued.

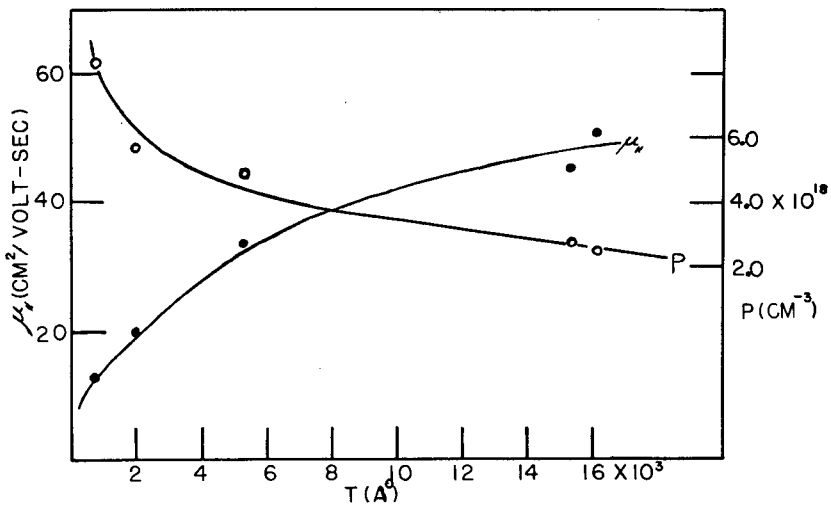

Fig. 4 - Hall mobility and acceptor concentration as a function of thickness

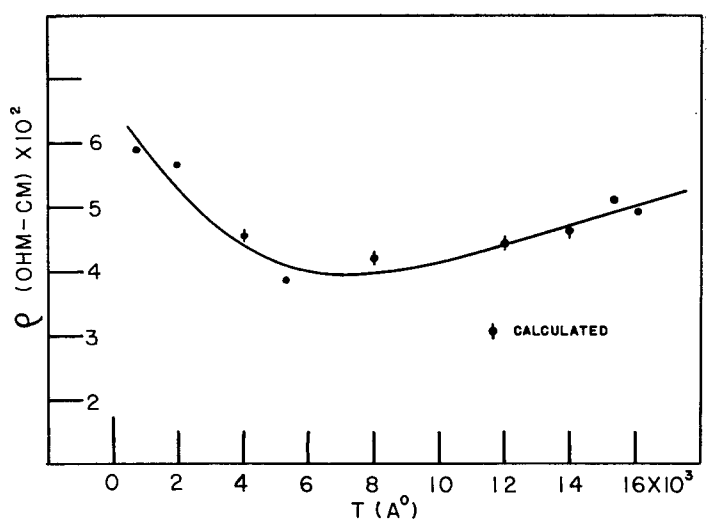

Fig. 5 - Resistivity as a function of thickness

UNCLASSIFIED

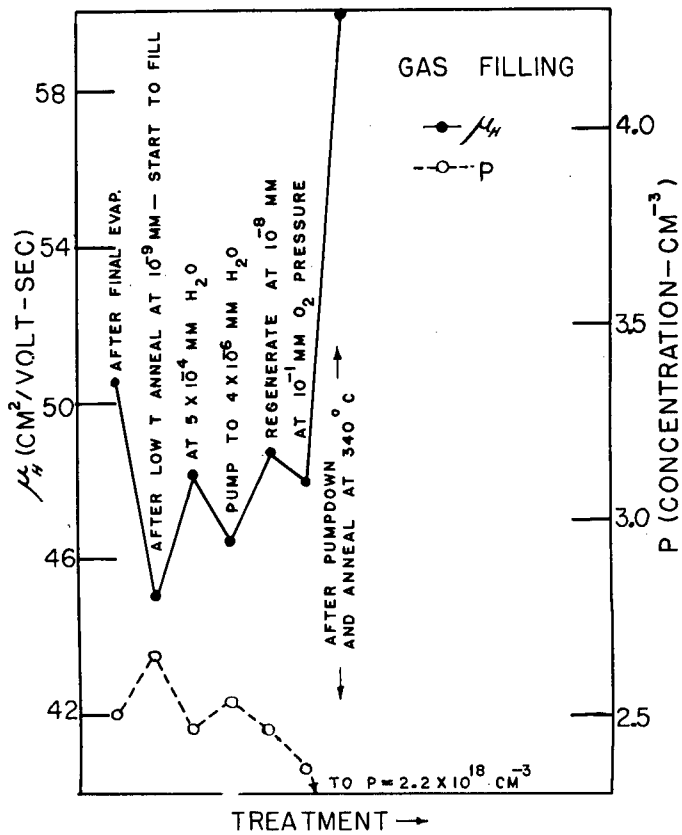

Fig. 6 - The effect of ambients of H_2O and O_2 on the mobility and concentration

There were a number of difficulties inherent in the present work which are now being investigated and which will be corrected in future measurements. First there is the effect of boron transfer, in a borosilicate glass system, during the initial stages of pump down. This has been reported by Law, et. al. (5) as the cause of p-type films on silicon. Presently we are using his "control conditions" to investigate methods of pump down in a borosilicate glass system which will allow no transfer of boron. Also in the case of bulk Ge there is a ubiquitous conversion of n to p at annealing temperatures of 800°C, for all except very highly doped samples. This phenomena is usually attributed to Cu in-diffusion. Since the Ge samples must be raised above 800°C to approximately 1200°C, during the evaporation, the cause of the conversion effects must be determined before the p character of the evaporated films may be unambiguously analyzed. Finally there are the questions of local pressure rises due to the evaporation, coupled with the low pumping speed of the 3 stage oil diffusion pump and 5 liter/sec vac-ion pump, the effect of back diffused oil vapor, and the reaction of the tungsten gun with the Ge samples. In answer to these objections, a new vacuum system has been designed which operates a 57 liter/sec 3 stage Hg diffusion pump, in parallel with a 75 liter/sec vac-ion pump. Since the backing pump in front of the Hg pump will be doubly trapped there should be present no back diffused oil or hydrocarbons in the high vacuum tube at any time. Also the factor of 10 increase in pumping speed should optimize low contamination conditions during evaporation. Finally the reaction of a Si-W system has indicated no p character at the Si-W interfaces, while the free surfaces, exposed in a borosilicate system, went strongly p type. Although one can't extrapolate this behavior to Ge, it seems likely that conversion effects, rather than a W-Ge reaction, are the cause of p character in Ge bulk.

[redacted]

It is strongly recommended that all aspects of this problem, as listed above, be continued as outlined since in order to utilize germanium in thin film device form the origin of these effects must be determined. In particular, the effects of boron transfer as well as other high vapor pressure materials, the effect of disorder diffusion as a possible cause of p character and finally the effects of conversion, all as related to the ultra-high vacuum measurements on Ge films.

BIBLIOGRAPHY

1. Davey, J.E., J. Appl. Physics, 32, 877 (1961)

2. Pokrowskij, J.E., Zh. tekh. Fiz. 24, 1229 (1954)

3. Eckart, F., and Jungk, G., Monatsber, Deut. Akad. d. Wiss. z. Berlin 2, No. 5, 266 (1960)

4. Kurov, G.A., Semiletov, S.A., and Pinsker, Z.G., Kristallografiya 2, 59 (1957)

5. Allen, F.G., Buck, T.M., and Law, J.T., J. Appl. Phys. 31, 979 (1960)

[redacted]

UNCLASSIFIED

CURRENT FLOW DUE TO MOTION OF CHARGED DISLOCATIONS

W. H. Vaughan
(Unclassified)

The Naval Research Laboratory (Solid State Division) has been concerned with the study of imperfections and the effects of imperfections on the properties of solids. These studies have emphasized optical, etch and X-ray techniques for gross imperfections. A sensitive light scattering apparatus has been built and is being used to study impurities in the alkali halides. A second very useful technique is a sensitive hardness test which has been used to study the motion of dislocations. The materials being investigated include a variety of water soluble crystals ranging from simple cubic alkali halides, both pure and containing various additives, and complex structures such as ammonium phosphate.

. . . . . FBM Staff

In recent years dislocations have been shown to be involved in a large number of structure-sensitive crystal properties. These properties include plastic deformation, creep, ductility, fatigue, fracture, recrystallization, and internal friction. Any increased knowledge about dislocations can be expected to throw light on processes that involve dislocations.

The alkali halides (Lif, NaCl, KCl, etc.) are ionic crystals that are transparent to visible light, can be easily grown in large single crystals of a high degree of purity, and can be cleaved into rectangular parallelepipeds with definite crystallographic faces. They are thus almost ideal crystals to use in studying the properties of dislocations. Within limits a crystal can be considered as a matrix in which occur certain imperfections such as interstitials, vacancies, or dislocations. The dislocations behave as entities whose properties are a function of the lattice spacing and the elastic constants of the crystal. Thus one can learn much about the properties of dislocations by working with a model crystal and use the results to predict the behavior of materials that are difficult to investigate.

The simplest and most extensively applied method of observing dislocations is the etch-pit method. This method can be applied to any crystal which can be cleaved to give crystallographic planes that can be etched or, like germanium, is hard and can be cut and polished without producing extensive damage. The alkali halides have been used in many investigations into dislocation hebavior. However, these investigations are limited to a maximum resolvable dislocation density of less than $10^8/cm^2$ for the optical microscope and less than about $10^{10}/cm^2$ for replicas in the electron microscope. The highest resolvable dislocation densities are obtained in transmission electron microscopy and here again the limit is of the order of $10^{11}/cm^2$ and it is applicable only on extremely thin specimens of the order of 500A°. There is thus a great need for a technique which can somehow characterize dislocation motion in the presence of a high density of dislocations. It will be shown in this report that the current flow from a plastically deformed crystal probably can be used as a tool to obtain insight into the behavior of one aspect of dislocations however high their density.

This report gives results that were obtained from crystals that were deformed either in straight compression at a constant strain rate or by cycling between fixed strain or fixed stress limits. It is concluded that while the induced charge was probably due to

[redacted]

charged dislocation jogs as suggested by Fischback and Nowick,* the origin of these jogs was due to cross-glide rather than intersection. This explanation fits all of the observations on charge flow, as well as the recent observations on dislocation motion by Gilman and Johnston.*

The electrical effect associated with the deformation of alkali halides has a long history. In 1928 Gyulia and Hartley† reported an increase in the conductivity of rock salt following plastic deformation. Stepanow†, while looking at the Gyulia-Hartley effect, observed a charge flow in the external circuit when no electrical field was applied. In 1934 Kassel† reported the possibility of decreases as well as increases in the conductivity of NaCl during deformation. In 1950 Seitz† interpreted the Gyulia-Hartley effect as the generation of vacancies by the motion of dislocations. At about this time Tyler† reported that the conductivity increase was twice as large for colored crystals as for uncolored crystals. Since the color centers are believed to be electrons trapped in negative ion vacancies, it was reasonable for him to suggest that some of the Gyulia-Hartley effect might be due to the generation of free electrons by dislocation motion.

Johnston† while investigating the conductivity increase of AgBr due to plastic deformation observed a decay in the measured conductivity with a very long recovery time. He interpreted his results as indicating the formation of disordered regions of low conductivity during plastic deformation. Burneister† investigated the effect of plastic deformation on the electrical conductivity of KCl containing large additions of $CaCl_2$ in the temperature range 230°C to 350°C and found a conductivity increase which was proportional to the initial deformation. He explained this in terms of the Mott† theory of turbulent hardening in which build-up of dislocations results in a conductivity increase, as well as work hardening.

Additional observations on alkali halides were reported in the work of Caffyn and Goodfellow‡ who found, "a change in conductivity associated with the process of homogeneous strain throughout the crystal." They also found, "the appearance of a potential at the electrodes apparently caused by stress inhomogeneities," Their work was interpreted as indicating some kind of impurity influence, since they observed no conductivity increase in any crystals from some sources. At about the same time, Fischback and Nowick made their excellent measurements on the transient electrical effect of the plastic deformation of NaCl. They investigated the temporary increase in the ionic conductivity and the deformation induced charge flow. Their results were interpreted as indicating that vacancies freed by dislocations gave rise to the conductivity increase, and that charged dislocation generated by intersection of dislocations were responsible for the charge flow.

The next work was the cyclic stressing of NaCl by Amelinckx, et al.,‡ in which the results were interpreted in terms of vacancy atmospheres about charged dislocations. In addition, there was the work of Camagni, et al.,‡ in which they determined an activation energy for the motion of freed vacancies at 0.45 ev as compared with 0.68 ev in undeformed crystals. They used the distorted regions about dislocations that had been considered earlier by other investigators to explain the discrepancy and finally there is the work of Rueda and Dekeyser§ in which they observed a charge flow associated with microindentations and concluded that the observed effect corresponds to the transport of negative charge by moving dislocations.

In further work, Vennik, et al.§ cyclically stressed crystals of NaCl and LiF by means of a vibrator with pulses of different duration and observed memory effect. That is, they

*See Bibliography (1 thru 5)

†See Bibliography (6 thru 13)

‡See Bibliography (14, 15, 16)

§See Bibliography (17, 18)

UNCLASSIFIED

found that if a crystal which had been first subjected to a series of pulses of constant amplitude and alternating polarity and then was exposed to increased amplitude, the new current pulses showed a sharp change in slope at the point corresponding to the maximum deformation of the previous cycle. This effect was observed independently at this Laboratory in a similar way and will be discussed later more fully.

EXPERIMENT

The charge flow was measured with a Keithley 610A Electrometer while compressing NaCl, NaCl + Ag, LiF, LiF + Mg, KCl crystal blocks in the Instron Tensile Tester. Except where otherwise mentioned, the crystals were all grown at NRL, cleaved, given a standard anneal of 700°C for two days, furnace-cooled at less than 1°C/min, and stored in a desiccator until used. Contacts were made with a silver paint after determining that the nature of the contacts did not affect the result. The only requirement was that contacts be thoroughly dry and this could be speeded up by the application of a stream of hot air. The crystals were compressed between glass plates, with metal lugs cemented onto the lower of these plates. These lugs were connected to the crystal by gold wires which were cemented to the contacts by silver paint. The electrometer was connected to the lugs.

RESULTS

The deformation-induced charge flow was investigated by compressing the end faces of relatively long crystal clocks ($\cong 0.4 \times 0.4 \times 2$ cm). In view of the random nature of the resulting current flow, electrodes were placed on all four of the lateral faces. It was hoped that in this way it would be possible to find some correlation between the mode of deformation and the charge evolution.

A differentiation between edge and screw dislocations can be made when one can observe the direction of the slip bands, by etching, for example. At moderate deformation $\simeq 2\%$, however, the surface is completely covered with etch pits and another method must be used to determine the principal directions of slip. Birefringence is very useful at this degree of strain. When the crystal, viewed between crossed polaroids, is so oriented that the slip bands show up as streaks of white against a black background one is looking parallel to the slip planes. This is sufficient to determine the slip plane or planes. With few exceptions, the majority of the crystals which birefringence revealed to have deformed in simple slip (i.e., along one set of parallel planes instead of all four that are equally stressed) showed the behavior that is illustrated in Fig. 1. The screw faces generally reached a peak first in the current flow and this peak was significantly higher than that for the edge faces. This result is compatible with most of the charge being carried by jogs in edge dislocations.

To investigate this effect more thoroughly, cycling about zero stress was applied. Since the Instron Tensile Tester was designed for tension or compression but not for a mixture of both, a slight modification was necessary. The compression load cell was "biased" by a load of about 10K gm to which was cemented the crystal. The crystal was also cemented to the top plates as shown in Fig. 2. This made it possible to cycle the load from 10K gm in tension to 10K gm in compression. These observations are in agreement with the work of Remant, Vennik, and Amelinckx on the cyclic stressing of alkali halide single crystals. However, because of the must greater strains that were attained in this experiment more information was obtained.

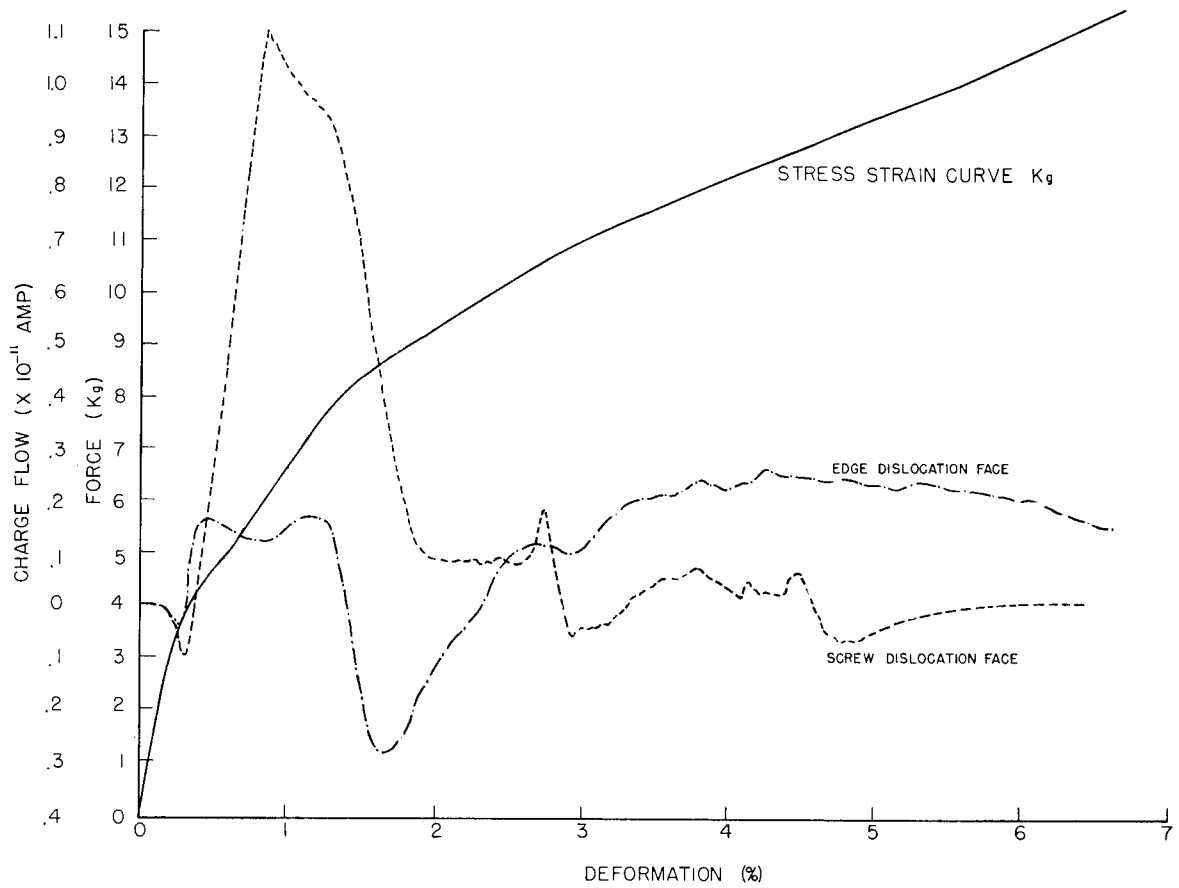

Fig. 1 - Typical results of simultaneous stress-strain measurements and current flow observations

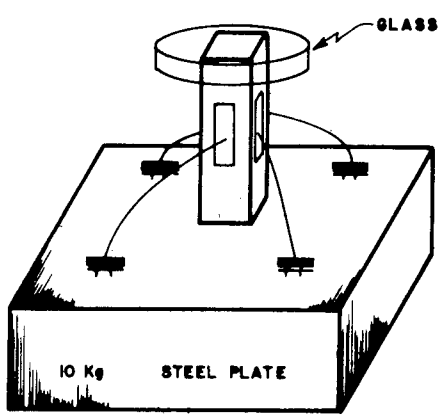

Fig. 2 - Arrangement for "biasing" load cell to enable it to record tension or compression on the crystal. The crystal was cemented to the steel plate and to the glass insulator on top. The insulator, in turn, was cemented to the crosshead of the tensile tester.

[redacted]

UNCLASSIFIED

The crystal was cycled between A and B with the charge flow as indicated in Fig. 3. When the load limits were changed to B and C, the result showed a large increase on the first 1/4 cycle of increasing compression and then the charge flow oscillated about a constantly decreasing curve that came down to the initial zero value. This behavior has been designated the memory effect, and can also be observed when the deformation is stopped at any place in the cycle. Figure 4 shows a typical result when the crystal was stopped at the highest compression end for two minutes. The subsequent current showed a large increase in the first quarter cycle at the low compression end and then oscillated about a curve that dropped back to zero. A symmetrical result is obtained if the deformation is stopped at the other end of the cycle. This effect would be dismissed as a transient if one were cycling at a high frequency.

The effect of doping, quenching, annealing, and surface treatments were investigated.

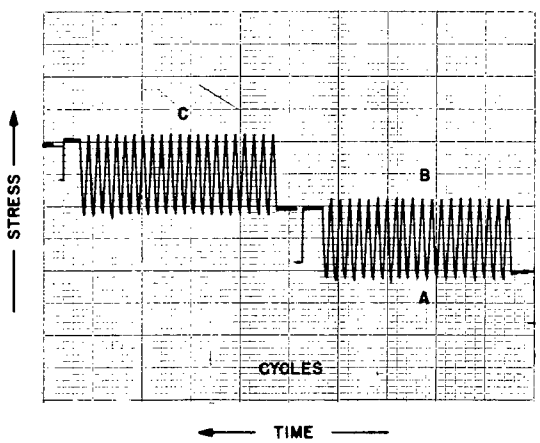

Fig. 3 - Part of stress-strain curve for a crystal cycled between load limits with a constant difference such that the lower and upper limits were increased in equal increments up to the yield point.

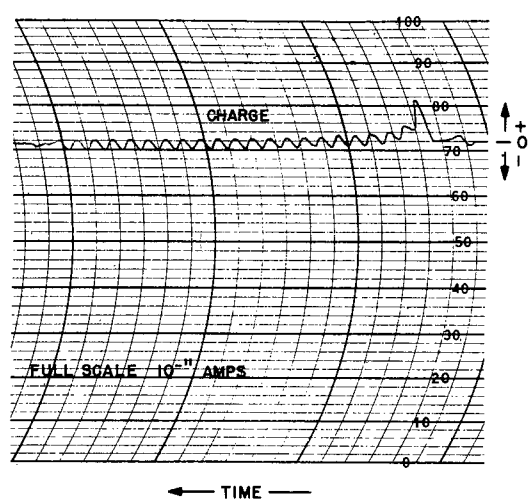

Fig. 4 - Typical charge flow after changing load limits

[redacted]

DOPING

Single crystals of KCl with Pb and with Ag, and of NaCl with Pb and Cd were deformed in compression. In all cases the addition of impurities increased the charge flow by at least an order of magnitude.

HEAT TREATMENT

Quenching these crystals showed the same result as had been obtained with undoped quenched crystals – a very low charge flow. Two single crystals of LiF and two single crystals of NaCl were quenched from 600°C into CCl_4 at room temperature. All crystals gave off charge at a much lower rate - 1/10 to 1/100 that of the corresponding unquenched crystal. Such quenching treatments could be expected to give the crystal a large number of dislocations which do not have atmospheres of point defects. Some 600°C quenched crystals were annealed at 400°C for 1 hour and furnace-cooled to room temperature. The latter treatment was applied to both NaCl and LiF, and resulted in deformation induced charge flows that were similar to that from crystals that had been quenched only. However, careful handling following deep etching and polishing of the surface in many cases give higher values than crystals that had been only quenched.

A Harshaw single crystal of NaCl was deformed in compression at a strain rate of 0.0025/min until a point was reached at which the charge flow was appreciably constant. This point was reached well past the yield point at a deformation of 2%. The sample was then removed from the Instron, cleaned of contacts and annealed for one hour at 300°C in air and then furnace-cooled. Contacts were again put on the sides and compression continued. The resulting charge flow was within 5% of the original value.

Crystals which had been subjected to heavy X-irradiation with hard X-rays 100 kv on a tungsten target were deformed and the charge flow was measured. It was found that, in general, X-irradiation with hard X-rays increased the charge flow by 1 to orders of magnitude. Etching these crystals showed that the slip bands were very narrow as would be expected in a hard crystal. Furthermore, the slip bands were narrower at the surface than inside which indicates that slip band broadening takes place all through the crystal rather than only at the surface.

SURFACE TREATMENTS

The surface treatments used were abrasion with a fine polishing cloth which resulted in the production of a high density of dislocation on the surface of the order of $10^8/cm^2$, four hours of X-irradiation at 10 kv and 35 ma with a chromium target which, on a single crystal of KCl, resulted in considerable hardening of the surface with but little penetration, and finally addition of surface active molecules such as stearic acid, citric acid, and butyric acid to the surface which resulted in a lowering of dislocation mobilities on the surface. A number of tests were made by subjecting one or more of the faces to a surface treatment and comparing its subsequent charge flow under compression with an intreated face. In other tests deformation was interrupted, the surface treatment was carried out and then deformation was resumed. The charge flow after treatment was compared with the charge flow before treatment. All of the surface treatment experiments, except abrasion, gave negative results. That is, surface treatments before deformation did not make a lateral face significantly different from the other lateral faces and surface treatments that interrupted the deformation did not change the rate at which charge was given off by any face. However, crystals which had been abraded on all four sides before deformation showed very low charge flow which was similar to that of quenched crystals And abrasion of one lateral face before deformation, for the nodes of slip which put edge dislocations on the adjacent faces, resulted in the abraded face getting a positive charge while the opposite face become negative.

UNCLASSIFIED

DISCUSSION

Studies made of the dislocation density as a function of the strain for MgO by Stokes, Johnston and Lee, for LiF by Gilman and Johnston, and in germanium by Patel and Alexander (and in Si-Fe by Guard and Low)* have shown that all of these crystals have essentially the same plastic behavior. That is, free dislocation loops that are somehow present initially in the crystal glide when the applied stress reaches their yield point, multiply after some cross-gliding, leaving behind a number of loops near the initial plane. The new loops glide, multiply, collide with each other and are either annihilated or become blocked, during which time the glide bands broaden and increase in dislocation density. The motion of dislocations within the band is slow and dislocations of both signs are present in each slip band. (Incidentally, this is one of the stumbling blocks in any dislocation-based explanation of the charge flow. If one has approximately equal numbers of dislocations moving in each direction in a slip band, now can dislocations carry any net charge.) At the edges of the band, the dislocations are free to move and cross-glide so that the band grows until adjacent bands overlap each other and the surface of the crystal is completely covered with dislocations. The difference between the plastic behavior of MgO and LiF is apparently due to the difference in hardness, the softest MgO behavior is very much like the hardest LiF while the softest LiF behaves much like NaCl. In general, the softer the crystal the broader will be the slip bands at a comparable strain.

We found much the same behavior with the charge flow although of course there is a great deal of scatter since the result depends so much upon the exact deformation. In general, pure KCl gave the lowest currents and the addition of impurities of any valence increased the results. Similar behavior was observed with NaCl and LiF; the harder crystal gave the higher current for comparable deformation. As shown on Fig. 5, the current would start out low, often change sign, reach a maximum near the yield point, then decrease rapidly at first, and then more and more slowly until fracture occurs. At large deformations (10-20%) the currents are so low (10^{-15} amps) as to be almost undetectable.

Since annealing a deformed crystal after its current has passed the maximum had has had no effect on the subsequent charge flow, the results cannot be explained in terms of vacancy atmospheres about charged dislocation lines. Then, too, the work of Rueda and Dekeyser and the earlier work of Fischback and Nowick indicates that there is a negative charge associated with dislocations that were nucleated by a high stress concentration. Therefore, an explanation which is in agreement with all of the recent work on the multiplication and motion of dislocations and the observations of deformation induced charge flow is as follows: Starting with an annealed crystal, all the old dislocations are immovable due to the presence of point-defect atmospheres. New dislocations on the surface, due to cleavage and handling, move when the stress reaches the yield point. These dislocations move into the crystal from the surface and multiply by cross-gliding to form bands. The process of cross-glide produces jogs in dislocations some of which, according to Seitz,† can be expected to be charged. The dislocations produced by cross-glide can be expected to be of both signs. Indeed, geometrical considerations indicate that any method of producing dislocations of both signs in equal numbers. However, since the original dislocations came in from the surface, the first pairs of dislocations produced by the multiplication process will give a net contribution in the same direction as the original dislocation – the dislocations of opposite sign have only a short distance to go before they leave the crystal. As a given slip band broadens there is more and more cancellation. From this point of view the peak would be expected to occur in the charge flow when the net dislocation motion in one direction is a maximum.

*See Bibliography (19 thru 23)

†See Bibliography (24)

[redacted]

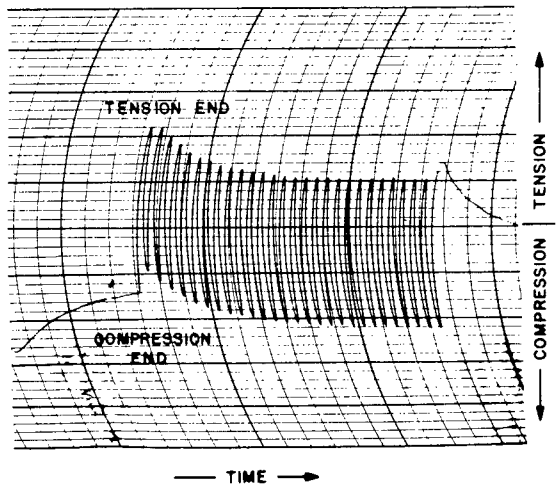

(a)

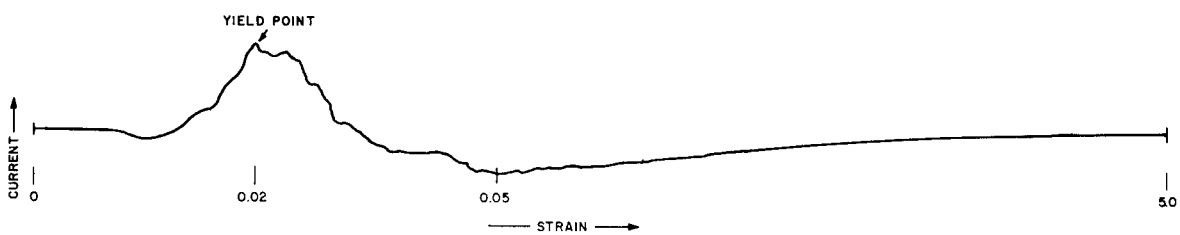

(b)

Fig. 5 - Common behavior of crystal held under a constant load and then cycled between tension and compression limits

From observations made of the currents from all four lateral faces and the mode of deformation from birefringence, which in the majority of crystals the larger currents came from faces that were at 45° to the burgers vector of the active dislocation, it seems likely that the charge is carried by jogs in edge dislocation.

The charged jogs probably are produced by cross-gliding which broadens the slip bands. Cross-gliding can take place on the surface or inside of a crystal. Surface cross-glide contributes only dislocations that move into the crystal while volume cross-glide gives dislocations which move in both directions in the slip band. However, the results on KCl with soft X-rays in which no effect was found indicate that the production of charged jogs probably rake place inside the volume.

A logical question is, "What role do vacancies play in the deformation induced charge flow?" This is reasonable because vacancies carry a charge in ionic crystals and since the elastic field about a dislocation can attract and move a vacancy. However, there is a great deal of evidence that "vacancy drag" does not play an important role in the charge flow. First, in the experiments with hard X-irradiation, the crystals give essentially the same currents immediately after X-irradiation or following an anneal at 250°C

UNCLASSIFIED

for one hour, which should have removed the excess vacancies produced by irradiation.* Second, the enhancement of the charge flow by additions of monovalent silver indicate that vacancies do not play much of a role in the process of deformation-induced charge. The most obvious effect of the silver additions was a hardening of the crystal with a resultant narrowing of the slip bands. Indeed any process which narrowed the slip bands were found to give higher charge flows.

Quenching and abrasion both give rise to high densities of mobile dislocations. Quenching strips the impurity atmosphere from old dislocations and makes them mobile, as well as producing a large number of new dislocations through thermal stresses. Abrasion gives rise to a high dislocation density on the surface. When only one lateral surface is abraded, subsequent deformation results in large numbers of dislocations moving away from that face to the other three lateral faces. Therefore the charge acquired by the abraded face is opposite to the charge carried by the dislocations. For this reason it was concluded that dislocations carry a negative charge in undoped NaCl. Therefore, when all four lateral faces are abraded or the crystal is quenched, the resultant low net charge flow is caused by the fact that approximately equal amounts of charge are carried in all slip directions.

If this interpretation is correct, one can expect to learn a great deal about the motion of charged jogs. At the present time there are good techniques for studying in a detailed way the behavior of dislocations when the density is low. At low strains 3%-4% in the harder crystals one can no longer resolve optically the etch pits in the slip bands and electron microscope replicas are not very well suited to dynamic studies.

The memory effect can be explained by the creep of dislocations containing charged jogs under a given stress. It would be very interesting to measure the memory effect as a function of temperature to obtain some kind of activation energy. The lack of change in the charge flow with annealing is puzzling and these experiments are being repeated.

*See Bibliography (25)

[redacted]

BIBLIOGRAPHY

1. Fischback, D.B., and Nowick, A.S., J. Phys. Chem. Solids 5, 302 (1958)
2. Gilman, J.J., and Johnston, W.G., J. Appl. Phys. 27, 1018-; -22 (1956)
3. Gilman, J.J., and Johnston, W.G., "Dislocation and Mechanical Properties of Crystals," John Wiley, New York, p. 116-164 (1957)
4. Johnston, W.G., and Gilman, J.J., J. Appl. Phys. 30, 129-144 (1959)
5. Johnston, W.G., and Gilman, J.J., J. Appl. Phys. 31, 632-643 (1960)
6. Gyulia, Z., and Hartley, D., Z. Phys. 51, 378 (1928)
7. Stepanow, A.W., Z. Phys. Sowjet, 4, 609 (1933, Z. Phys. 81, 560 (1933))
8. Kassel, M., Z. Phys. 90, 287 (1934)
9. Seitz, F., Phys. Rev. 80, 239 (1950); Advances in Phys. 1, 43, (1952) Symposium Held at Pocono Manor, J. Wiley and Sons (1950)
10. Tyler, W.W., Phys. Rev. 86, 801 (1952)
11. Johnson, W.G., Phys. Rev. 98, 1777 (1955)
12. Burneister, Z. Phys. 148, 408 (1957)
13. Mott, N.F., Phil. Mag. 43, 912 (1952)
14. Caffyn, J. E., and Goodfellow, F.L., "Nature," No. 4486, Vol. 176 p. 878 (1955)
15. Amelinckx, S., Vennik, J., and Remant, G., J. Phys. Chem. Solids, 11, 170 (1959)
16. Camagni, P., Chiarotti, G., and Manara, A., Phys. and Chem. Solids, 17, p. 165 (1960)
17. Rueda, F., and Dekeyser, W., Phil. Mag. 6, 63 p. 359 (1961)
18. Vennik, J., Remant, G., and Dekeyser, W., Phil. Mag. Vol 6 No. 68, p. 997 (1961)
19. Gilman, J.J., Plasticity, p. 43 (1960) Pergamon Press, edited by Lee and Symonds
20. Guard, R.W., and Low, J.R., Acta Met. Vol. 7, p. 171 (1959)
21. Johnston, W.G., and Gilman, J.J., J. App. Phys. Vol. 30, p. 129 (1959)
22. Stokes, R.J., Johnston, T.L., and Li, C.H., Trans. Amer. Inst. Mech. Engrs. Vol. 215, p. 431 (1950)
23. Patel, J.R., and Alexander, B.H., Acta Met. Vol. 4, p. 385 (1956)
24. Seitz, F., Rev. Mod. Phys. 23, p. 328 (1951)
25. Kobayashi, K., Phys. Rev. 41, p. 107 (1957)

[redacted]